DETECTION OF GLUCOSE USING PRINTED MICROFLUIDIC DEVICES

OPTIMIZATION OF PRINTED MICROFLUIDIC DEVICES FOR THE ELECTROCHEMICAL DETECTION OF GLUCOSE

By ZEXI WANG,

A Thesis Submitted to the School of Graduate Studies in Partial Fulfillment of the Requirements for the Degree Master of Applied Science

McMaster University

MASTER OF APPLIED SCIENCE (2024)

Hamilton, Ontario, Canada (School of Biomedical Engineering)

TITLE:	Optimization of Printed Microfluidic Devices for the Electrochemical Detection of Glucose
AUTHOR:	Zexi Wang BS (Medical Sciences), University of Western Ontario, London, Canada
SUPERVISOR:	Dr. Changqing Xu and Dr. Zhiyi Zhang
NUMBER OF PAGES:	xiv, 107

Lay Abstract

This thesis presents a novel material that can mimic the properties of paper. The proposed material can be easily printed onto carbon electrodes to form a printed microfluidic device. The fabrication process is cheap and scalable for mass production. The material can transport fluids via capillary action much like paper can, and can also handle glucose detection using electrochemical methods. The results show that the printed microfluidic devices could detect glucose with high sensitivity and low detection limits, making them potentially useful for medical diagnostics. This technology also successfully integrated other microparticles into its composition to boost its electrochemical performance and improve its sensitivity. This novel material offers a cost-effective, easy-to-produce, and reliable alternative to current methods, with potential application in point-of-care testing.

Abstract

Paper-based microfluidic devices have been a promising device platform for point-of-care diagnostic applications. It is known for its cost-effective and simple nature. Various analytes, such as metabolites, electrolytes, and pathogens, have been quantified in various applications. One of the key advantages of paper-based devices is the inherent property of capillary flow, which allows for the transport of fluids without the need for external pumping. However, since their discovery, applications of paper-based microfluidics have become increasingly complicated. Using expensive materials or complex surface modification to push the device's performance to its limits. Many have lost sight of what made paper-based microfluidic devices attractive in the first place. Despite these advances and recently reported devices having extremely low sensitivity, none have been commercialized, like the first testing strips. This thesis presents a novel material that can mimic the properties of paper. The proposed material can be easily printed onto carbon electrodes to form a printed microfluidic device. The fabrication process is cheap and scalable for mass production. Unlike existing devices, the proposed material allows for a completely new area of design and optimization. This technology successfully demonstrated that it could similarly transport fluids to paper and the electrochemical detection of glucose. The results show that the printed microfluidic devices could detect glucose with high sensitivity and low

detection limits, making them potentially useful for medical diagnostics. The material was also integrated onto commercially available screen-printed electrodes and shown to improve performance. The composition of the material is flexible and capable of being tuned for specific needs. For example, semi-conductive microparticles can be integrated for an improvement in electrochemical performance. The results show that the printed microfluidic devices offer a cost-effective, easy-to-produce and reliable alternative to current methods, with potential application in point-of-care testing.

To my father,

mother and brother

Acknowledgements

I would like to sincerely thank my supervisors, Dr. Chang-qing Xu, for his confidence and trust, which allowed me to start on this journey, and Dr. Zhiyi Zhang, for his patience, guidance, and support throughout my research. It has been an honor and a privilege to have the opportunity to learn so much from both of you. I would also like to thank my Supervisor Committee member, Dr. Ravi Selvaganapathy for meeting with me and addressing the many questions I encountered during my research.

Table of Contents

List of Figures

List of Tables

Abbreviations

μPAD	Microfluidic Paper-Based Analytical Device
μPED	Microfluidic Paper-Based Electrochemical Device
Ag/AgCl	Silver/Silver Chloride
PET	Polyethylene Terephthalate
KCl	Potassium Chloride
$K_3[Fe(CN)]_6$	Potassium Ferricyanide
Al_2O_3	Alumina or Aluminum Oxide
ZnO	Zinc Oxide
GOx	Glucose Oxidase
PVA	Polyvinyl Alcohol
DMSO	Dimethyl Sulfoxide
PVAc	Polyvinyl Acetate
DIP	Di(propylene Glycol) Methyl Ether Acetate

LOD Limit of Detection

Declaration of Academic Achievement

The following is a declaration that the research described in this thesis was completed by Mr. Zexi Wang and recognizes the contributions of Dr. Chang-qing Xu and Dr. Zhiyi Zhang. Zexi Wang contributed to the study's design and was responsible for the fabrication of the device, experimental protocol, data collection, data analysis and the writing of the manuscript. Dr. Chang-qing Xu and Dr. Zhiyi Zhang offered help with the inception of the study, the design of the study, and the review of the manuscript. Dr. Zhiyi Zhang also contributed to the collection of images used in the thesis

Chapter 1

Introduction

1.1 Paper-Based Microfluidic Devices

A widespread paradigm shift in the past decade has been intersectionality. Combining various disciplines resulted in the introduction of novel subfields and continuous technological advancement. For example, combining the traditional fields of chemistry, biology, physics, and engineering has led to the rise of new microfluidics and electrochemistry application areas. Likewise, the two have become increasingly linked, making it difficult to treat them as separate entities (Rackus et al., 2015). Microfluidics is the study and manipulation of small volumes of fluids in the ranges of μL to pL. To satisfy these conditions, the devices are often planar substrates bearing enclosed channels with lengths, widths, and heights on the scale of micro- to nanometer. Microfluidics is a unique field of study that was popularized in the early 1990s because fluids behave in a completely different way when dealing with micro- and nanoscale compared to the macro world. The most critical parameters for the microfluidic phenomena include Reynold's number (Re), Capillary Number (Ca), and

Péclet number (Pe) (Rackus et al., 2015).

$$Re = \frac{\rho l v}{\mu} \tag{1.1.1}$$

$$Ca = \frac{\mu v}{\gamma} \tag{1.1.2}$$

$$Pe = \frac{v l}{D} \tag{1.1.3}$$

where:

ρ - fluid density

l - length of the system

v - fluid velocity

μ - dynamic fluid viscosity

γ - surface tension

D - coefficient of diffusion

In microfluidic devices, these parameters are low, meaning viscous forces will dominate inertial forces, interfacial forces will dominate viscous forces, and diffusion will dominate convection. Ultimately, this means that fluids in a microfluidic system will behave laminarly rather than turbulent (Rackus et al., 2015). This phenomenon is an important characteristic of microfluidic systems as it allows for more controlled separation or mixing of fluids. Microfluidic platforms can be classified into various categories based on channel design and material selection. For example, paper-based microfluidics, channel-based microfluidics, and digital microfluidics (Rackus et al., 2015). There are also many alternative classifications, but the focus will be

on paper-based microfluidics. Paper is usually made by pressing together cellulose fibers, which can be separated from raw sources such as wood and cotton by chemical or mechanical pulping. The cellulose is cross-stacked and interconnected during manufacturing, generating a hierarchical porous structure (Cate et al., 2014). Compared with conventional microfluidic systems, this hierarchical porous structure keeps the Reynold's number low for laminar flow but still allows fluid to diffuse through capillarity (Rackus et al., 2015). The movement of fluids through paper is described by the Lucas-Washburn equation (Shen et al., 2019):

$$x(t) = \sqrt{\frac{\sigma t r \cos\theta}{2\eta}} \tag{1.1.4}$$

where:

x - distance moved by the fluid front under capillary pressure

t - time

σ - liquid-air surface tension

r - average pore radius of the paper

θ - liquid-fiber contact angle

η - viscosity

Paper-based microfluidics is an alternative scheme for traditional miniaturized fluid handling where the liquid samples are passively pumped by capillary action through a paper substrate (Gong and Sinton, 2017). The Whiteside group popularized this method in 2007 (Martinez et al., 2007), and many products have become widely available to consumers utilizing this method, for example, pregnancy tests, the COVID-19 antigen test, and glucose test (Yamada et al., 2017). Paper-based

microfluidics is popular because of the very low cost, ease of fabrication, flexibility, biodegradability, and the passive diffusion of liquid via capillary action (Radhakrishnan et al., 2022). For these reasons, there has been a particular interest in using paper-based microfluidics for point-of-care diagnostics in resource-limited settings (Cate et al., 2014) (Costa-Rama and Fernández-Abedul, 2021).

Paper microfluidics are implemented by forming hydrophobic/hydrophilic patterns to leverage the inherent properties of paper, such as its porosity and capillary action, to create a fluidic pathway (Anushka et al., 2022). On common technique is wax printing, where patterns are printed onto the paper using a wax printer, followed by heating to melt the wax, penetrating the paper to hydrophobic barriers that define the microfluidic channels. Another approach is photolithography, which involves coating the paper with a photoresist, exposing it to UV light through a mask to create the desired pattern, and then developing the paper to wash away the unexposed areas, leaving behind hydrophobic regions. Furthermore, inkjet printing, flexographic printing and plasma treatment are among the numerous strategies that have been utilized to generate paper-based devices (Li et al., 2012) (Alahmad et al., 2023).

Although paper is a unique substrate for containing liquids in specific areas and can control fluid flow without the use of external power, the above characteristics are of limited use in the analytical sense if no other functionalities were incorporated (Shangguan et al., 2018). For application purposes, several detection techniques have been proposed (Zheng et al., 2021). Colorimetric assay is a common type of detection method used with μPADs. In a colorimetric assay, a chemical reaction produces a color change that has an intensity proportional to the concentration of analyte in the sample (Li et al., 2012). This can be instrument-free, with the color

changes being detected with the naked eye, or semiquantitative results can be obtained by comparing the color produced to a color calibration chart. Quantitatively, a technique known as digital image colorimetry can be applied. Where a digital image of the assay is analyzed using software such as ImageJ, MATLAB or Adobe Illustrator. Another detection method frequently used is electrochemical. This method explores the usage of electrochemistry techniques for a more quantitative analysis of the sample.

Electrochemistry has historically been a branch of chemistry investigating electron transfer kinetics, with applications in semiconductors, batteries, and electrochemical sensors (Mettakoonpitak et al., 2016). The latter application has seen increasing attention because of various advantages, including inexpensive instrumentation, miniaturization, mass scalability, and high sensitivity. The systems are typified by the uses of inexpensive potentiostats (a control circuit that applies electric potential and measures small currents) and electrochemical cells that are easily screen printed (a highly scalable manufacturing technique that is low cost). These advantages are one of the driving factors behind the popular and now ubiquitous paper-based electrochemical glucose microfluidic devices.

The electrochemical phenomenon of interest is the reduction-oxidation reaction. It is often measured using a cell comprised of three electrodes: (1) a working electrode (WE), where the redox reactions of interest occur and are measured; (2) a counter electrode (CE) is controlled by a potentiostat to set the WE potential and balance the current, and (3) a reference electrode (RE) that provides feedback of the WE potential to the potentiostat (Mettakoonpitak et al., 2016). The WE and CE are in direct contact with the solution being studied, and the RE is often in indirect contact

via a conductive salt bridge. Multiple characteristics can contribute to the design of the electrodes, for example, size, geometry, material, and surface topography (Cate et al., 2014). While electrodes traditionally have had dimensions on the order of millimeters, with the advancements in microfluidics and micromachining, the concept of "microelectrodes" and "nanoelectrodes," where micrometer and nanometre scale electrodes are achievable. Electrodes with these dimensions allow for the detection of even smaller currents in the ranges of picoamperes to nanoamperes, rapid responses to the changes in applied potential, and ultimately, the more efficient and sensitive detection of ultralow concentration of analytes from ultralow sample volumes.

When the electrode is charged, and it encounters the ions in solution, an electrical double layer of ions (5-20 nm thick) is formed at the surface (Bard and Faulkner, 2000). The layer closest to the electrode is the inner layer (Stern Layer), where excess charge is balanced by a fixed equal number of oppositely charged ions. The second layer is the diffuse layer, which contains a group of oppositely charged ions with concentrations decreasing exponentially as a function of distance from the inner layer. There is a constant drop in potential from the electrode surface to the stern layer. The potential at the stern layer is referred to as the zeta potential, which gives the exponential decreasing nature of the charges with distance (Rackus et al., 2015). In an electrochemical process, the analyte moves from bulk solution to the electrical double layer by one (or more) of three methods: (1) diffusion, the movement due to the concentration gradient between the bulk solution and the electrode surface region; (2) migration, the movement due to the potential gradient between the electrode surface and the bulk solution, and (3) convection, forced movement through mechanical forces (Mettakoonpitak et al., 2016).

As mentioned previously, the analyte participates in a redox reaction because of the electric potential that is measured between WE and RE. The electric potential and the concentrations of the analyte being oxidized or reduced can be determined using the Nernst equation:

$$E = E^0 + \frac{RT}{nF} \ln \frac{C_o}{C_r} \tag{1.1.5}$$

where:

E^0 - "standard" potential for the reaction

R - universal gas constant

T - temperature

n - number of electron transfers involved in the reaction

F - Faraday's constant

C_o, C_r - concentration of species being oxidized and reduced respectively

The simplest form of electrochemical sensing, potentiometry, where the Nernst equation is used to discern C_o/C_r in a passive system with no outside potential applied. In addition, there are many other electrochemical techniques, but voltammetry and amperometry are most used within microfluidic applications

Voltammetry is an extensively used technique, and it can probe the reversibility of the system. The electric potential is applied between the WE and CE, resulting in a current. But unlike amperometry, the potential is varied as a function of time, usually forming a cyclic pattern. Using this method allows for the association of each step (oxidation and reduction) with a peak current (i_p). The relationship between peak current and the scan rate of electric potential (v) is given by Randles-Sevcik

equation (Rackus et al., 2015):

$$i_p = (2.69 \times 10^5) A C D^{\frac{1}{2}} n^{\frac{3}{2}} v^{\frac{1}{2}} \tag{1.1.6}$$

where: i_p - peak current

A - electrode area

C - concentration of analyte in bulk solution

D - diffusion coefficent

n - number of electron transfers involved in the reaction

v - scan rate

Due to the analytes being regenerated, the peak current can be further enhanced by running multiple cycles (Elgrishi et al., 2017). Since electrochemical techniques are sensitive to the analyte's flow rate, considering the sample's flow rate through paper is another important design characteristic.

Paper	Material	Thickness (μm)	Volume/Area (μL/cm^2)	Flow (mm/min)
Whatman Grade 1 Chr	Cellulose	180	9	4.3
Whatman Grade 3MM Chr	Cellulose	340	15	4.3

Whatman Grade P81	Cellulose with phosphate groups	200	7	3.2
Whatman Grade DE81	Cellulose with diethylaminoethyl groups	230	7	4.2
Whatman Grade GF/F	Glass fiber	420	21	

Table 1.1: Features of common paper types employed as substrate for paper-based microfluidics. Adapted from (Amor-Gutiérrez et al., 2022)

Amperometry, as the name suggests, is an electrochemical analysis technique that measures the current while a constant external electric potential is applied between the WE and CE. The current is recorded as a function of time. Because electron transfer can only occur at the electrode, the current at the WE is proportional to the movement of the analyte to the electrode surface (Rackus et al., 2015). For instance, in a system with only diffusion and no convection or migration movement, the flux of the analyte will depend on the concentration gradient of the analyte. Initially, only the analyte near the double layer is depleted, resulting in a high current. As the analytes deplete, more analytes will flow from the bulk solution. Eventually, the region of reduced analyte will extend further into the solution, and thus, the concentration gradient declines with time, which causes the current to decline. The

current observed in amperometry will follow Cottrell's Equation shown below (Rackus et al., 2015):

$$i = \frac{nFAc_j^o\sqrt{D_j}}{\sqrt{\pi t}} \tag{1.1.7}$$

where:

i - current

n - number of electrons

F - Faraday constant

A - area of the planar electrode

c_j^o - initial concentration of the reducible analyte

t - time

For the proper healthcare of people, rapid, accurate, and minimally invasive diagnostic tools are in high demand (Xu et al., 2022). The current standard of care requires off-site analyses, where the sample is transported to a laboratory for analysis, which can significantly delay in the therapeutic decision and miss the timing window for certain preventative measures (Yoo and Lee, 2010) (Zhang et al., 2021). The primary benefit of POC diagnostics is the dramatic speed advantage over conventional techniques because it takes place on-site (Kulkarni et al., 2022). An example of this is continuous glucose monitoring (Manasa et al., 2022). This not only allows for the early detection of biomarkers, but also earlier treatment and precautionary measures to take place, preventing disease progression to a more serious state. Paper-based microfluidics, also known as paper-based analytical devices (μPADs), is the perfectly suited device for these situations, fully utilizing its advantages. Among many others, cellulose paper is flexible, biocompatible, eco-friendly, inexpensive, available, and easily modified chemically and physically, and there is a lack of necessity for an external

pump (Gutiérrez-Capitán et al., 2020). Its flexible nature enables a 3D element in the form of origami (Colozza et al., 2021). Electrochemical detection approaches show certain advantages, such as their small size, low cost, low power consumption, high selectivity, and sensitivity, as well as the availability of a large number of measuring techniques, which can be adapted to different analytical detection mechanisms (Costa-Rama and Fernández-Abedul, 2021).

1.2 Electrochemical Sensing in Paper-Based Microfluidics

As mentioned previously, the term paper-based microfluidics was first introduced by Martinez et al. (2007). However, they chose to implement μPAD as a colorimetric assay. The analyses are realized by visually comparing the color change of the reaction spots before and after loading analytes. The analyte concentration can then be quantified using image analysis software easily accessible on a smartphone or a handheld optical colorimeter. The downside of such a technique is that inaccuracies can arise for multiple reasons. For example, when the color change is heterogeneous due to a small sample, this can limit the ability of the software to quantify the quantity. Another bottleneck of colorimetric detection is its sensitivity to ambient light conditions (Ataide et al., 2020).

Dungchai et al. (2009), merged the concept of electrochemical detection with μPADs, creating microfluidic paper-based electrochemical devices or μPEDs. The channels were created using photolithography, and carbon electrodes were printed using screen printing techniques. Electrochemical methods offered higher detection

sensitivity and low cost. The selectivity can also be adjusted by varying electrochemical parameters and/or electrode materials for different applications. A key component of the selectivity is due to the enzyme. Enzymes are biological catalysts able to accelerate any chemical reaction, not being consumed in the process nor being part of the final product. Enzymes decrease the activation energy of reactions, showing greater specificity. Enzymes typically only act on one specific substance, making it a great marker for differentiating even between different stereoisomers of one compound. A critical step for designing enzymatic electrochemical biosensors is immobilizing said enzymes on the surface of the microfluidic device.

Adsorption is the simplest method of immobilization. It is generally done by dissolving the enzymes in a buffer solution and then contacting a solid surface. The bonds formed in this immobilization are weak, such as Van der Waals' forces and electrostatic or hydrophobic interactions (Amor-Gutiérrez et al., 2022). The main drawback is that any change in the conditions of the medium, such as pH, temperature, and enzyme desorption, affects the stability of the biosensor. Adsorption can be carried out in three different ways: (1) physical adsorption, where the enzymes are directly deposited on the surface of the electrode; (2) electrostatic interactions, when the enzymes are immobilized onto a charged surface; and (3) retention in a lipidic microenvironment, using Langmuir-Blodgett technology (Amor-Gutiérrez et al., 2022). Immobilization of enzymes can also be carried out inside a three-dimensional matrix, where the enzymes, mediators, and additives are all simultaneously deposited on the surface of the electrode. The enzyme activity is preserved since the biological elements are not modified. The entrapment is mostly done by electrochemical polymerization, where a current or potential is applied to an electrode with a mixture of

the enzyme and monomer in a way that physically incorporates the enzyme within the polymer network. Polymers such as polyaniline and polypyrene are most used for conducting polymers, but other matrices, such as polysaccharide-based gels, are also viable options. Other methods, such as cross-linking, embedding, affinity, and covalent reactions, can also be used to immobilize the enzyme, each with advantages and disadvantages (Amor-Gutiérrez et al., 2022).

In the development of μPED, apart from design and patterning, electrode fabrication is another critical step since, ultimately, electron transfer is the phenomenon of interest, and the electrode surface determines the analytical characteristics of the device. Various methods have been reported for the fabrication of electrodes on paper platforms. Film-based electrodes are usually employed for paper-based enzymatic biosensors to determine glucose. Thick film methodology (μm-thick layer) employs inks; a popular method is screen printing or inkjet printing (Tortorich et al., 2018). Pencil drawing and painting are also viable options. However, a thin-film methodology, such as gold-sputtered electrodes, also makes it possible to obtain an nm-thick layer. Below is a table highlighting some of the advances in paper-based microfluidics over time.

Author	Year	Substrate	Sample Volume/Media	LOD of Glucose	Fabrication Method	Electrochemical Detection Method	Novelty

(Dungchai et al., 2009)	2009	Glucose, Lactate, Uric Acid	Human serum Sample	0.21 mM	Photo-lithography for channels, screen printed electrodes	Cyclic voltammetry	First paper-based electrochemical glucose biosensor
(Nie et al., 2010b)	2010	Glucose, Lactate, Uric Acid	Artifical Urine	0.22 mM	Wax printing or Photo-lithography for channels, screen printed electrodes	Chrono-amperometry, anodic stripping voltammetry	
(Nie et al., 2010a)	2010	Glucose, Choles-terol, Lactate, Alcohol	Human whole blood	26 mg/dL	Wax printed channels, screen printed electrodes	Amperometry	Testing designed test strips vs commercial device, 0.014 per strip not better LOD than commercial

(Lankelma et al., 2012)	2012	Glucose	Urine	N/A	Wax printed or Photolithography for channels, platinum sputtered electrodes	Amperometry	Utilization of flow injection analysis
(Zhao et al., 2013)	2013	Glucose, Lactate, Uric Acid	Artificial urine	0.35 mM	Wax printed channels, screen printed electrodes	Chronoamperometry or Cyclic voltammetry	Multiplex detection + custom open source, handheld, portable potentiostat
(Noiphung et al., 2013)	2013	Glucose	Whole blood	N/A	Wax dipping for channels, screen printed electrodes	Cyclic voltammetry	Prussian blue modified non-integrated screen printed electrodes

(Kong et al., 2014)	2014	Glucose	Human whole blood	0.1 mM	screen printed electrodes	Differential pulse voltammetry	Graphene, polyaniline, Au nanoparticles, GOx modified screen printed carbon electrodes
(Li et al., 2015)	2015	Glucose	Human serum Sample	59.5 μM	Wax patterning for channels, stencil printed electrodes	Cyclic voltammetry and chrono-amperometry	Zinc Oxide nanowires were grown on top of the electrode
(Li et al., 2016)	2016	Glucose	Human blood samples	0.05 mM	Laser printed channels, electrodes were drawn by graphite pencils	chrono-amperometry	Origami design, 3D paper-based microfluidic

(Yao and Zhang, 2016)	2016	Glucose, Uric Acid	Real Urine Sample	0.35 mM	wax screen printing	Cyclic voltammetry	Improved screen printing, where patterning and electrode printing happen consecutively
(Parrilla et al., 2017)	2017	Glucose	Human serum Sample	0.03 mM	Platinum sputter electrodes	potentiometry	Nafion immobilization of GOx
(Cánovas et al., 2017)	2017	Glucose	Blood	N/A	Platinum sputter electrodes	Potentiometry	Fully integrated, compact, portable and disposable wireless paper-based potentiometric system, utilizing the Nafion immobilization from the previous paper.

(Li et al., 2017)	, 2017	Glucose	Human serum Sample	1 mM	Wax pen and conductive ink pen	Cyclic voltammetry and chrono-amperometry	Developed pen-on-paper-based microfluidic (draw the entire design)
(Chaiyo et al., 2018)	2018	Glucose	Human blood serum	0.67 μM	Wax printed channels, screen-printed electrodes	Cyclic voltammetry	First non-enzymatic electrochemical detection of glucose with cobalt phthalocyanine, graphene and an ionic liquid
(Lamas-Ardisana et al., 2018)	2018	Glucose	Commercial soft drinks	0.33 mM	Diluted UV screen-printing ink for patterning, carbon and Ag/AgCl for electrodes	Amperometry	Novel screen-printing ink for patterning, fully fabricated using screen printing

(Cinti et al., 2018)	2018	Glucose	Whole blood	0.17 mM	Wax- and screen-printing	Cyclic voltammetry and amperometry	Developed prussian nanoparticle paper -¿ reagent-less electrochemical POC device
(Wu et al., 2019).	2019	Glucose, PBS, BSA	Solution	0.32 mM	Wax screen printing	Cyclic voltammetry and chrono-amperometry	dual colorimetric and electrochemical detection in a 3D device
(Fava et al., 2019)	2019	Glucose	Urine	0.03 mM	Craft and cut for channels, screen printed electrodes	Cyclic, square wave, and differential pulse voltammetry, chrono-amperometry	16-channel multiplex assay

(Cao et al., 2020)	2020	Glucose	Human sweat and blood	0.025 mM	Photo-lithography for channels, screen printed electrodes	Cyclic voltammetry and chrono-amperometry	Novel 3D design, prussian blue deposited reduced graphene oxide-tetra-ethylene pentamine modified working electrode
(Sinha et al., 2020)	2020	Glucose	Human blood	0.02 μM	N/A	Cyclic voltammetry and chrono-amperometry	Oxygen-deficient $W_{18}O_{49}$ nanorod bundles for non-enzymatic glucose detection
(Kant et al., 2021)	2021	Glucose	Blood serum	10 μM	Inkjet printed paper electrodes	Cyclic voltammetry	Gold-nano particles ink as a non-enzymatic electrochemical sensor

(Niamsi et al., 2022)	2022	Glucose	Blood plasma	24.5 μM	Screen printed graphene electrode	Cyclic voltammetry	Ionic liquid, graphene electrode modified with MXene, Prussian Blue, GOx and Nafion

Table 1.2: History of Paper-Based Electrochemical Devices

It can be seen in Table 1.2 that each reported device uses a unique combination of fabrication, electrochemical detection methods, and sample media. In summary, the development of paper-based electrochemical biosensors can be divided up into different "generations", depending on how the enzyme glucose oxidase is used (Wang, 2008). Starting with the first generation, their principle is based on using oxygen as a co-substrate, producing H_2O_2 as the enzymatic reaction product, which is measured. This had several issues, such as the electrochemical monitoring of HO requires high operating potentials, which can affect the selectivity due to the high probability of interferences, i.e., other electroactive species that can also be reduced at those high potentials (Adeel et al., 2020). During the second generation, they overcame the high potential limitation by using redox mediators as co-substrates, which ensure efficient electron transfer at lower potentials and are regenerated on the surface of the electrode. Different electron mediators, such as ferrocene, ferrocyanide, cobalt phthalocyanine, and methylene blue, are among the most common. During the third generation, they did not need mediators since they are based on the direct transfer between the enzyme and the surface of the electrode at very low operating potentials.

Lastly, in the fourth or current generation, they are enzyme-free sensors in which the glucose is directly oxidized on the electrode surface. Although numerous enzyme-free sensors for glucose have been reported, mainly using electrocatalytic nanostructures, enzymatic glucose sensors are still preferred due to their biocompatibility (Amor-Gutiérrez et al., 2022).

1.3 Research Objective

In November 2023, Zhang and colleagues proposed a microfluidic device printed using functional materials that can form interconnected pores (Zhang et al., 2023). The printed devices can transport fluids by capillary action in the same fashion as paper-based microfluidic devices and have demonstrated compatibility with both colorimetric and electrochemical detection methods. A similar performance was obtained by copying the device designs of Dungchai and Whiteside's group (Dungchai et al., 2009) (Nie et al., 2010b). The fabrication process was only screen printing. It is simple, cost-effective, and scalable. Looking at the history of μPEDs, this has rarely even been done, with the most similar being in 2018, where the entire μPED was fabricated through screen printing, but paper was still the substrate (Lamas-Ardisana et al., 2018). Another instance was more recent, in 2020 there was a case of a self-powering pH sensitive silver pump that can also sense glucose, copying paper's inherent nature for passive fluid flow (Gentile et al., 2020). This research presented a solution to common limitations in μPEDs, such as difficulty of printing electrodes on paper and the resolution or design constraints of the channel. Another trend, as shown in Table 1.2, is modern PEDs have become increasingly complex with complicated surface modifications and expensive fabrication procedures, which deviated

from the original appeal of PEDs in the first place. This research addresses some of these challenges by developing an alternative to paper-based microfluidics. In the following thesis, the works of Zhang and colleagues will be built upon. The printed microfluidic material was optimized for electrochemical performance, and different microparticles or modifications were integrated to better understand the material or technique.

1.4 Thesis Organization

This thesis consists of five chapters. The first chapter, the introduction, gives a literature review on the topics of microfluidics and electrochemistry, the history of electrochemical detection in paper-based microfluidic devices, the motivation, and an overview of the thesis. The second chapter describes the fabrication process of the printed microfluidic device, the experiment preparation, and the testing procedure. The relevant equipment and chemicals employed are also introduced in this chapter. Chapter three presents and discusses the experimental results of the microfluidic devices printed with alumina-based materials. Comparisons between these results and reported papers are included in this chapter. Similarly, chapter four presents and discusses the results for devices printed with semi-conductive materials. This chapter discusses the requirements for optimal electrochemical performance for the printed microfluidic device. Chapter Five contains a conclusion based on the experiments from this study, limitations, and recommendations for future work.

Chapter 2

Experiment Methods

2.1 Chemicals

The printed microfluidic device has two components. One is the electrode; the other is the microfluidic layer. The working and counter electrodes are printed using carbon ink (ECI 7001 E&C) purchased from Loctite (Westlake, OH, USA) and silver conductor ink (Ag 5025) from Dupont (Wilmington, DE, USA). The reference electrode was printed with Ag/AgCl ink from Kayaku Advanced Materials Inc. (Westborough, MA, USA). Polyethylene terephthalate PET (ST 505) films were purchased from Tekra (New Berlin, WI, USA) and used as the primary substrate for the screen-printer. The microfluidic layer underwent several stages of optimization. The initial formulation comprised of dimethyl sulfoxide (DMSO), fully hydrolyzed polyvinyl alcohol (PVA) (MW60000), fumed silica (0.007 μm), fluorosurfactant and aluminum oxide (Al_2O_3) microparticles (Zhang et al., 2023). DMSO, PVA, and fumed silica were purchased from Millipore Sigma (Oakville, ON, Canada), while the fluorosurfactant and Al_2O_3 were purchased from Dynax (Pound Ridge, NY, USA) and Skypring

Nanomaterials Inc. (Houston, TX, USA) respectively. The first optimization step was adjusting the binder and solvent combination from DMSO/PVA to di(propylene glycol) methyl ether acetate (DIP)/polyvinyl acetate (PVAc). Then, the combination of DMSO with 87-89% hydrolyzed PVA was tested. All binders and solvents were purchased from Millipore Sigma. The Al_2O_3 microparticles were also replaced or only partially replaced with zinc oxide (ZnO). Carbon Black from Graphene Supermarket (Ronkonkoma, NY, USA) was tested in various ratios to the Al_2O_3 and ZnO microparticles. The microfluidic ink was also tested without any fumed silica. Potassium chloride (KCl), potassium (III) ferricyanide ($K_3[Fe(CN)_6]$), phosphate buffered saline, 3-aminopropyltrimethoxysilane, dextrose and glucose oxidase (from Aspergillus niger, 159579 U/g) (GOx) were purchased from Millipore Sigma and used for in the electrochemical experiments.

2.2 Microfluidic Channel Formulation and Optimization

First, PVA was dissolved in DMSO at an elevated temperature and constant stirring to make an 18% PVA master solution. The temperature was kept constant at 150^{o}C to prevent the solution from burning, and stirring was kept at a speed that would not generate air bubbles. After the PVA had dissolved, the solution was left to cool before making the microfluidic material. DMSO was weighed out in a plastic cup, and surfactant was added drop by drop. The mixture was vortexed for 30 seconds and manually spread onto PET with a scoopula. The surfactant was added to reduce the surface tension and allowed the material to spread well onto the PET. This

preliminary test also ensures that the material will spread well when printing on the PET later. The next step was adding the 18% PVA. Depending on the amount of microfluidic mixture, an extra drop or two of surfactant was added to accommodate the extra DMSO within the PVA solution. Sufficient PVA was added such that there were only 8% PVA by solid mass in the final mixture. Excess PVA would be stored at room temperature for later use. Fumed silica and Al_2O_3 were added based on the ratios left by the previous student. After adding the remaining components, the mixture was speed mixed at 2300 rpm/740 torr for 6 minutes with 30 seconds of ramp up and downtime in the SpeedMixerTM FlackTek Inc. Al_2O_3 was further mixed with a mechanical mixer if the mixture was not homogenous enough after the speed mix. Mixtures prepared on a different day would be speed mixed at the same setting before printing. Additional DMSO was added to achieve optimal mixture viscosity and ensure ease of printing. Prototype printing would be done by manually spreading the material over PET, mimicking the screen printer, and left to dry on a hotplate at 120^{o}C. The prototype would be visually inspected for imperfections to ensure the material was ready to print, and water was dropped on the microfluidic material to observe the flow. This was the initial production procedure, but several steps were taken to optimize the microfluidic formula and the entire methodology (Zhang et al., 2023).

To start, the DMSO to PVA ratio was adjusted such that the final PVA concentration was 3%. Various electrochemical experiments were conducted on devices printed using the 3% PVA formula, which will be discussed in detail later. The mixing process was also simplified to speed mixing for two cycles after adding the fumed silica and Al_2O_3. Mechanical mixing was completely removed from the procedure

because there were several instances where mechanical mixing caused the material to be more heterogeneous, and unwanted residue from the mixer was incorporated into the microfluidic. A common phenomenon observed with the PVA master solution was its gelation. This gelation was due to the high crystallinity of the fully hydrolyzed PVA, allowing it to physically crosslink with each other when the solution had cooled down (Bercea, 2024). This gelation reduced the viscosity of the PVA solution, leading to chain effects downstream of the production process. Not only did the gelation make mixing the materials more difficult and uneven, but it also made the printing and cleaning process more troublesome. Various solutions were tested, but new problems were also introduced. For example, the PVA master solution was replaced one-for-one with PVAc dissolved in DIP. Using the same formula, the microfluidic film made with the PVAc formula had a noticeably weaker structure and could not handle the mechanical stresses during printing. This was especially true for the 3% formula, although the 8% formula naturally provided more structure because of more binder. But another problem arose, which was that PVAc was more hydrophobic than PVA, and swapping the PVA with PVAc meant the water droplet no longer spread into the microfluidic and formed a bead instead (Squillace et al., 2020). This was problematic because the whole purpose of the microfluidic channel was to transport the solution in a controlled manner. Without it, the electrochemical experiments could not have been completed. Partially hydrolyzed (87-89%) PVA in DMSO was also trialed. Despite the gelation being resolved, the partially hydrolyzed PVA structure was susceptible to being dissolved in water, making it unsuitable for testing because all solutions used for the experiments were water-based (Aruldass et al., 2019). Ultimately, fully hydrolyzed PVA remained the primary binder for most

devices mentioned below. However, if gelation was observed, an extra step was added where the master solution was reheated to break down the bonds in PVA that caused the gelation before usage. Another issue arose particularly during winter, where the same amount of fumed silica would make the microfluidic material more viscous and affect the printing process mentioned later.

2.3 Device Fabrication

An ASYS EKRA X1-SL semi-automatic screen printer (ASYS group, Dornstradt, Germany) was used for printing, and the substrate was PET film. Four differently patterned 200-mesh stainless steel wire screens were used to print the various microfluidic materials and electrodes. Each screen was designed based on printing material and device components. Multiple variations of the simple designs proposed by Whiteside et al. and Dungchai et al. were adapted for the screen (Nie et al., 2010b). From Whiteside's straight channel design, two microfluidic channel widths (4mm, 2mm) and two electrode widths (4mm, 2mm) were incorporated. Additionally, a 1mm electrode was combined with the 2mm microfluidic channel, giving a total of 5 different devices. From Dungchai's multichannel design, the microfluidic channel had two different widths (3mm and 2 mm) and 1mm wide electrodes (Dungchai et al., 2009). On each print, five devices with each straight channel combination and 3 copies of each multichannel design. The distance between the screen and the substrate was approximately 2.4 mm. The devices were printed with a 75 Shore A polyurethane squeegee with a 65^o attack angle. A pressure of 3 bar was applied to the squeegee, and the print speed was 30 mm/s. The separation speed was set to 0.5 mm/s. The

low separation speed and high squeegee pressure were found to be necessary for better print quality and ease of pushing the material through the mesh screens. The first layer printed was the Ag conductor ink that will be underneath the working and counter electrodes. This helps reduce the resistance of the electrode, making current travel easier. Carbon ink was used as received for the working and counter electrodes. Commercial Ag/AgCl ink was printed on the film using a 200-mesh polyester screen to form reference electrodes. Before printing the reference electrode, the flood bar on the screen printer was covered with tape to prevent it from oxidation. Finally, two layers of microfluidic material were printed over the electrode after proper alignment. See Figure 2.1. for a schematic of the sequence during printing. Each layer was dried at 120^{o}C for 5-10 minutes, with the final microfluidic layer drying for longer at 10-20 minutes. Initially, the double microfluidic layer was of the same material to give the device more structure. However, later prints used the 3% PVA material for the first layer and 8% PVA material on top. These devices featuring this "hybrid" microfluidic channel were tested. After each material, the squeegee, flood bar, and screen were removed from the printer for deep cleaning to prevent residue ink from clogging the pores in the mesh. Hot water was used to clean the microfluidic material (Zhang et al., 2023).

A symptom of fumed silica increasing the viscosity mentioned previously was noticed during printing, where the material would dry up quickly and adhere to the screen instead of passing through to the PET film. This affected the number of devices that could be printed, and the material spread was uneven for each device. To reduce the gluiness, additional DMSO was added to the material, and the fumed silica was reduced, both of which were not ideal because the PVA concentration would be

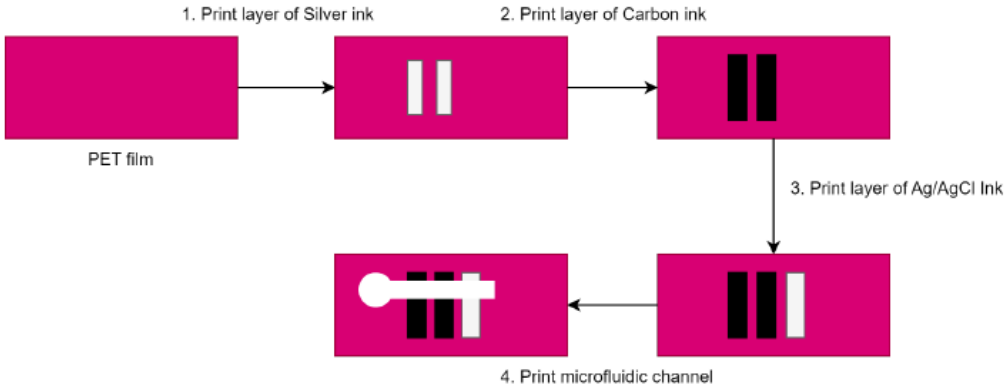

Figure 2.1: Schematic of ink sequence during device printing

changed. This phenomenon only appeared during the winter, and the main difference between the summer and the winter was the humidity. It was hypothesized that the lack of moisture led to an elevated association with the solvent due to prolonged storage of the fumed silica in a not-sealed environment. Therefore, humidity was a primary suspect, and introducing moisture was a potential solution. Fumed silica and Al_2O_3 would be left in a humidity chamber overnight before usage. Alternatively, Al_2O_3 was exposed to steam treatment for 5 minutes before usage. However, neither showed better results than leaving a humidifier inside the printing chamber during printing.

2.4 Device Characterization

The surface morphology of the printed microfluidic channels was characterized using a Hitachi scanning electron microscope (SEM). Pictures for various devices were taken. Resistance for the working electrodes in each device design was taken. A demonstration of the electrochemical application of the printed device was done using

the Princeton Applied Research PARSTAT 2263 potentiostat (AMETEK Scientific Instrument, Oakridge, TN, USA) with cyclic voltammetry. In cyclic voltammetry experiments, 6 μL of 1 mM potassium ferricyanide dissolved in 0.5 M KCl and 0.1 M PBS buffer (pH 7.4) was spotted onto the channel's inlet and allowed to spread through the channel. The experiments were performed between a potential of 0 V and 1 V at scan rates ranging from 25 to 400 mV/s. Experimental data was saved into a notebook and transferred to Excel for further examination. Follow-up data analysis included plotting the average cyclic voltammograms at each scan rate and the average anodic peak current relative to the square root of the scan rate (Zhang et al., 2023).

2.5 Glucose Detection Experiment

Glucose detection can be done through chronoamperometry, which is an electrochemical technique that measures the current generated from the redox reaction between GOx and glucose coupled with potassium ferricyanide. Two different potentiostats were used due to one of the machines malfunctioning. The PARSTAT 2263 and the CH Instruments CHI600D electrochemical analyzer. (Austin, TX, USA) were used to conduct the chronoamperometry experiments. The chronoamperometry experiments were performed using a step potential of 400 mV. The glucose samples ranging from 0 to 25 mM were prepared in 0.1 M PBS buffer at pH 7.4 and allowed to mutarotate overnight before use. An immobilization solution was later implemented using 1% 3-aminopropyltrimethoxysilane (APTMS) in 95% ethanol (Lee et al., 2018). The 1 μL of the solution was spotted on the detection zone, and the device was heated to 120^{o}C for 10 minutes. Then, 1 μL of enzyme solution was added directly to the top

of the microfluidic channel that covered the working electrode and allowed to dry at room temperature. Afterward, 6 μL of glucose sample was added to the channel inlets and allowed to travel through the whole channel (within 1 minute). For the multichannel design, the device was cut into 3 even sections, but the experimental procedure remained the same. The print device was taped to a flat ledge, allowing easy contact with the potentiostat clips. This also ensures the device was leveled and the sample does not flow due to gravity. The measurement was performed within 5 minutes after the channel was fully wetted. Data was transferred to Excel for further analysis. The average chronoamperometric curves for 0, 5, 10, 15, and 25 mM glucose were plotted. A calibration plot was made using the glucose concentration as a function of the current taken at 30 seconds. Taking the slope of the calibration plot and the standard deviation of the blank, the limit of detection (LOD) was estimated using Equation 2.5.1.

$$LOD = \frac{3.3 \times \mathrm{S}tandardDeviationofBlank}{\mathrm{S}lopeoftheCalibrationCurve} \tag{2.5.1}$$

Data for bare electrodes with no microfluidic layer was also collected as a comparison target to prove the benefit of the microfluidic material. Figure 2.2 depicts a graphic overview of the experimental procedure for chronoamperometry (Zhang et al., 2023).

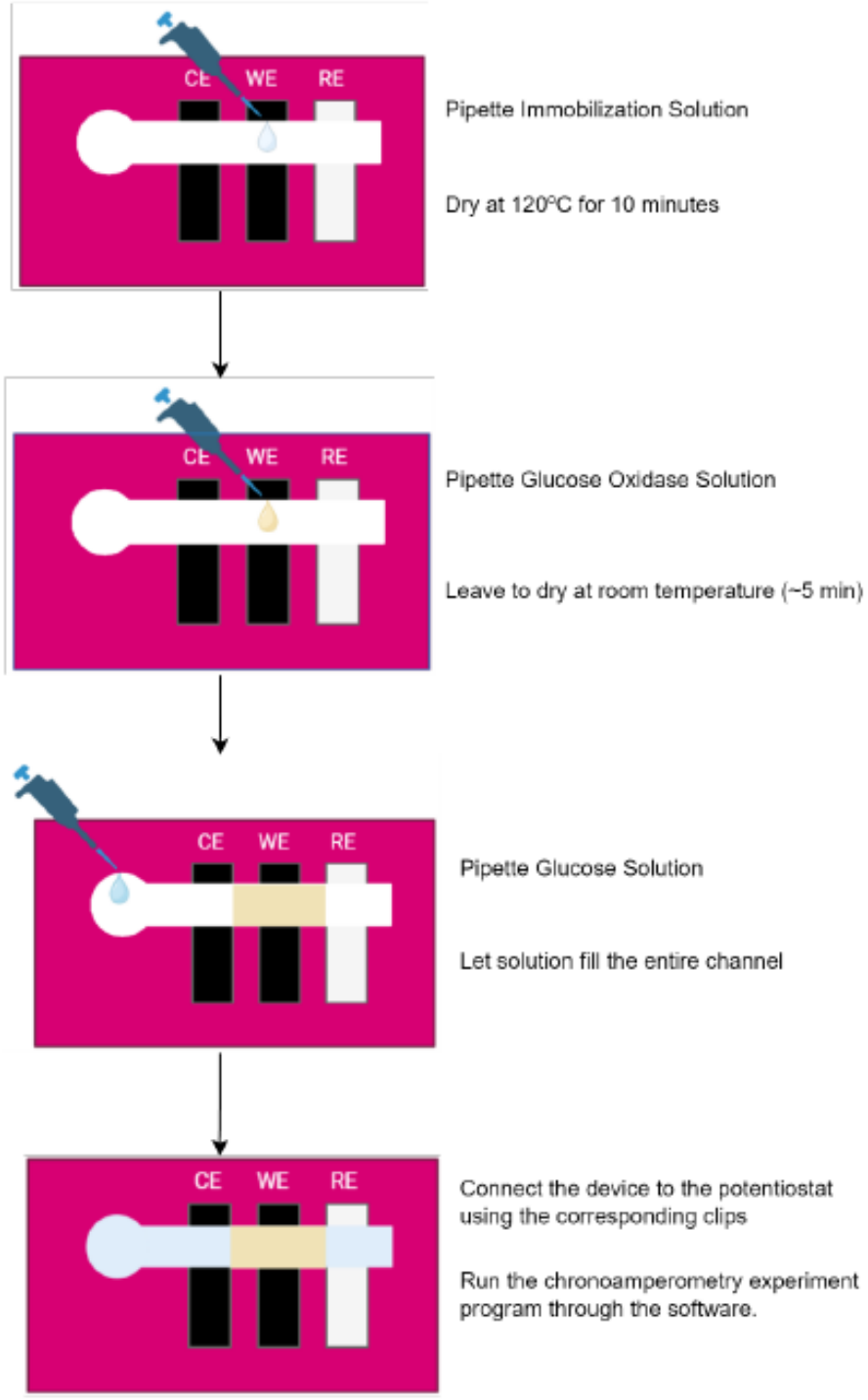

Figure 2.2: Schematic flow chart of the chronoamperometry experiment for electrochemical detection of glucose using the straight channel devices

2.6 Commercial Device Testing

Commercially available screen-printed electrodes were purchased from Metrohm DropSens (Llanera, Asturias, Spain). The device features an electrode configuration comparable to the multichannel design printed in-house and comprised of similar materials as well. The working and counter electrodes were carbon, and the reference electrode was silver. The device also had a wider detection zone with a bigger working electrode surface area and silver for the contacts. Due to the size of each device, the microfluidic layer was manually printed following a procedure mirroring the prototype printing mentioned previously. The commercial devices were tested using chronoamperometry with and without the microfluidic layer using the same procedure highlighted in section 2.4

2.7 Microfluidic Microparticle Changes

To further push the performance of the device, another change was made to the microfluidic material, where the main material was swapped from Al_2O_3 to a more conductive ZnO. Following the optimized procedure, enough ZnO was added to accommodate the same amount of volume as the Al_2O_3 used in the original 3% PVA formula. Additionally, various ratios of Al_2O_3 and ZnO were made. Similar combinations were made with Al_2O_3 and carbon black. At this time, a new problem surfaced where the material's viscosity was significantly affected, and it was unclear if the issue's root came from the newly incorporated ZnO and carbon black. Despite using the same formula, the fumed silica started to cause the material to be more gelatinous than normal. Therefore, mixtures without fumed silica were made.

Other modifications to the printing process included printing microfluidic pads (micropads) directly over the electrode rather than the entire channel. The micropads were printed using ZnO, Al_2O_3 with ZnO, and ZnO with carbon black. A new screen was designed specifically for this step. However, alignment issues led to missing sections being manually painted using a brush and ink. The idea of the micropads was to mimic the concept of surface modification of the electrodes. A double-layered 8% PVA channel was still printed over the micro pads to allow fluid transport.

Another difference when printing ZnO and Al_2O_3 was the fact that cracking was observed for ZnO, specifically over top of the carbon electrodes. This was due to the surface chemistry and particle solvent interaction differences between the two materials, where the surface tension prevented spreading, and after the DMSO was dried, the material cracked. ZnO, being more polar, is more likely to interact with the polar solvent, leading to higher surface tension (Kołodziejczak-Radzimska and Jesionowski, 2014). Al_2O_3 is amphoteric and tends to form aggregates with itself, which does not impact the surface tension (Nanja et al., 2020). Therefore, the amount of surfactant added in the original formula, which was suitable for Al_2O_3, was incompatible with ZnO. Plasma treatment was done after printing the electrodes and before printing the micropads in the Diener Atto Plasma Cleaner (Ebhausen, Germany). The plasma treatment removes hydrogen from the surface and attaches oxygen-containing species, generating a higher energy surface and allowing the material to spread more easily. Furthermore, plasma treatment has improved carbon electrodes' electrochemical properties (Kava and Henry, 2021) (Osaki et al., 2024). This was verified using in-house printed multichannel electrodes.

Chapter 3

Results and Discussion for Alumina Based Microfluidic Channels

3.1 Device Structure and Performance

The first printed devices had carbon ink electrodes with silver underneath and an Ag/AgCl reference electrode. The microfluidic channel was a double-layer alumina and fumed silica-based material bound together by 8% PVA. The figure below is a picture of the devices printed on a sheet of PET film. The design for these devices was heavily influenced by Whiteside's and Dungchai's research (Dungchai et al., 2009) (Nie et al., 2010b). Copying their designs isolates the parameters that can impact the performance of the printed microfluidic channel and experimental procedure. Initially, even the experimental procedure was copied; however, for better performance, several steps were added as optimizations (Nie et al., 2010b). Variations to the original design

were also made to investigate the impact of the electrode and channel width on the signal.

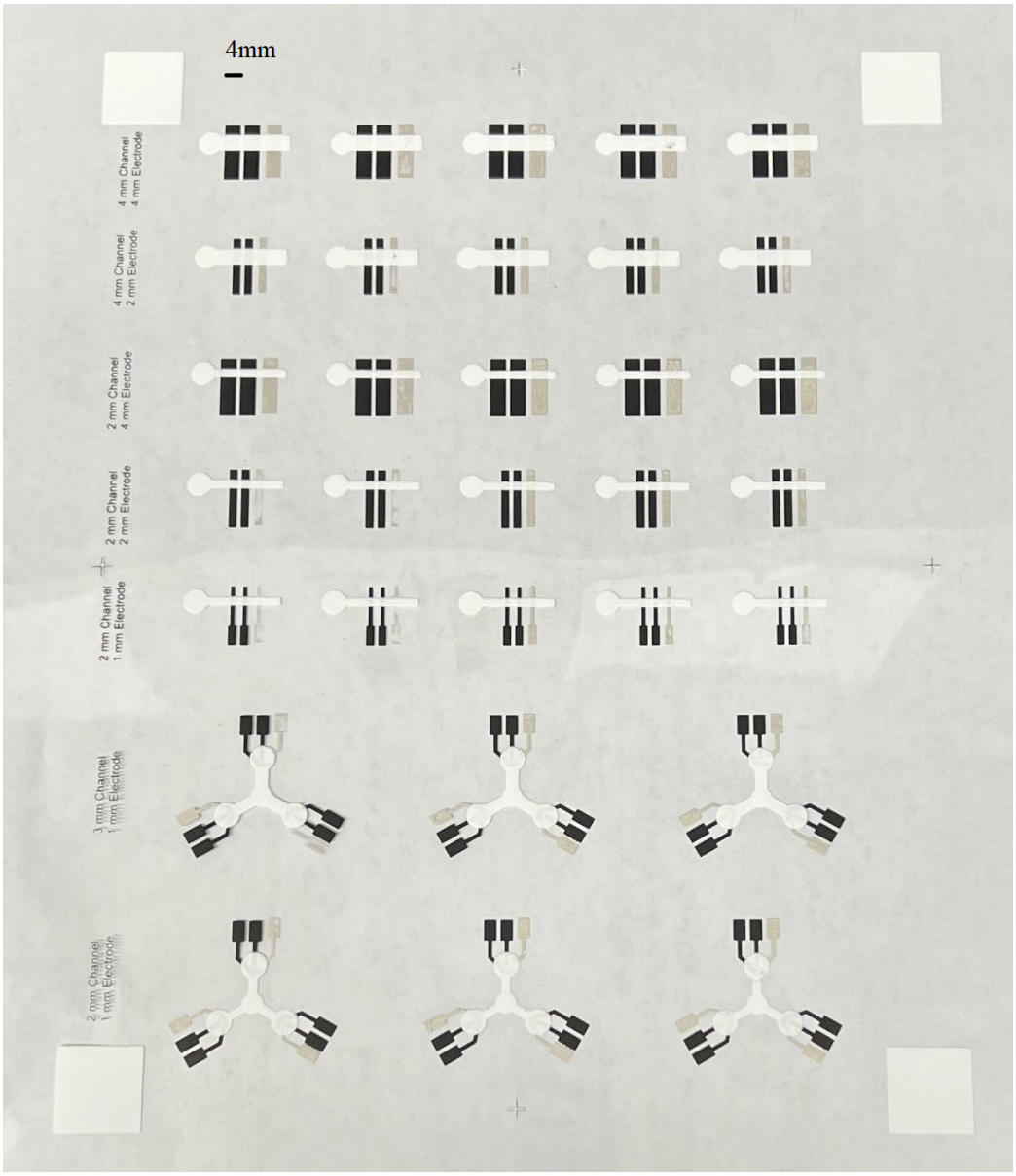

Figure 3.1: Optical Picture taken of a sheet of printed microfluidic devices on PET film on top of a blank paper background

As shown in Figure 3.1, multiple devices can be printed at once, demonstrating

the ability to scale and mass produce these devices. The versatility of the different channels and electrode sizes or designs is another advantage of this technology. Starting from the top, the first row are devices with 4mm wide channels and electrodes. These are the exact same design as Whiteside's devices (Nie et al., 2010b). Next are the 4mm channel and 2mm electrode devices. Then, 2mm channel by 4mm electrode, 2mm by 2mm, and 2 mm by 1mm for the last row of straight channels. For simplicity, each device will be codenamed based on its design; for example, 4M4E would designate the 4mm channel using a 4mm electrode. Starting in the 6th row, the multichannel design was copied from Dungchai's devices (Dungchai et al., 2009). Lastly, the final row is the same electrodes, but the channel width is 2mm instead of 3mm. Cyclic voltammetry tests were only performed on the 4mm-by-4mm device. Six μL of 1 mM potassium ferricyanide dissolved in 0.5 M KCl and 0.1 M PBS buffer (pH 7.4) at scan rates of 25, 50, 100, 200, and 400 mV/s, as seen in Figure 3.2 below. Devices were all visually screened for any imperfections in the electrodes or microfluidic channel before testing to ensure a fair result.

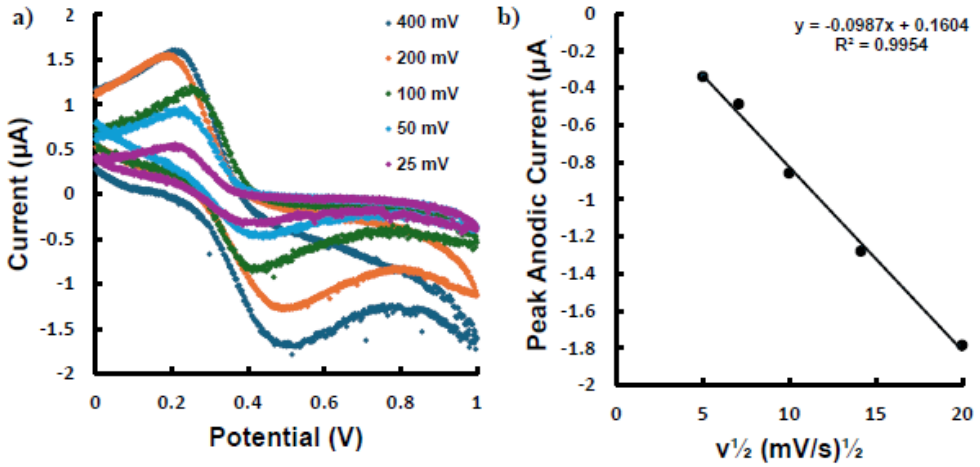

Figure 3.2: a) Cyclic Voltammograms of 1 mM $K_3[Fe(CN)_6]$ at 25, 50, 100, 200 and 400 mV/s. b) Anodic peak current plotted as a function of the square root of the scan rate.

The redox reaction of potassium ferricyanide is a reversible process, as indicated by the shape of the cyclic voltammograms seen in Figure 3.2A. This makes it a suitable mediator for the detection of glucose. The standard redox potential for potassium ferricyanide is approximately 0.36 V versus Ag/AgCl reference electrode (Rock, 1966). Looking at the anodic and cathodic peak currents for the 400-mV curve, the midpoint between the two peaks is 0.358 V. This value is close to the standard potential for the ferricyanide/ferrocyanide redox couple, indicating that the measurement is for the correct reaction. However, there were still discrepancies. For the 25-mV curve, the midpoint between the two peaks was only 0.31 mV, slightly less than the standard potential. A possible explanation for this result is the slow scan rate and the small concentration of potassium ferricyanide used. Due to the equilibrium nature of the redox reaction, although the optimal potential has not been reached, some redox will still occur due to the applied potential. This could lead to the phenomenon where all

the redox reactions had already finished before the standard potential. Additionally, the shift in the peaks at higher scan rates is likely due to the nature of the device. The microfluidic layer on top of the electrode meant the material could semi-prohibit the potassium ferricyanide from accessing the electrode. Furthermore, potassium ferricyanide can readily diffuse within the printed microfluidic channel as shown by the linearity of Figure 3.2B, it is satisfying the Randles-Sevcik equation(1.1.6) (Elgrishi et al., 2017). The diffusion-controlled system will have a steeper concentration gradient and less time to diffuse, creating an increased gap between peaks when scan rates increase. The results described above align with the findings of the earlier investigation (Nie et al., 2010b). There were some device artifacts, such as a noisy signal, and several solutions were trialed to resolve this problem. The sensitivity of the potentiostat was lowered, and the clips were changed from alligator teeth to flat contacts for better connectivity, but neither proved to be a complete solution. Retesting was done using spare devices to confirm the accuracy of the results, but unless the noise was entirely corrupting the data, this artifact was mainly ignored. Another artifact was the current measurement was negative. This made comparisons with various literature difficult. Therefore, all current values were multiplied by -1 during data analysis to correct for this fact.

Chronoamperometry was performed for all other devices except for the 2mm by 1mm device. A minimum of 2 replicates were obtained for each measurement. As previously mentioned, potassium ferricyanide is reduced to potassium ferrocyanide as a byproduct of GOx's glucose oxidation to gluconolactone. Then, during chronoamperometry, the electrochemical oxidation back to ferricyanide can be monitored as a current.

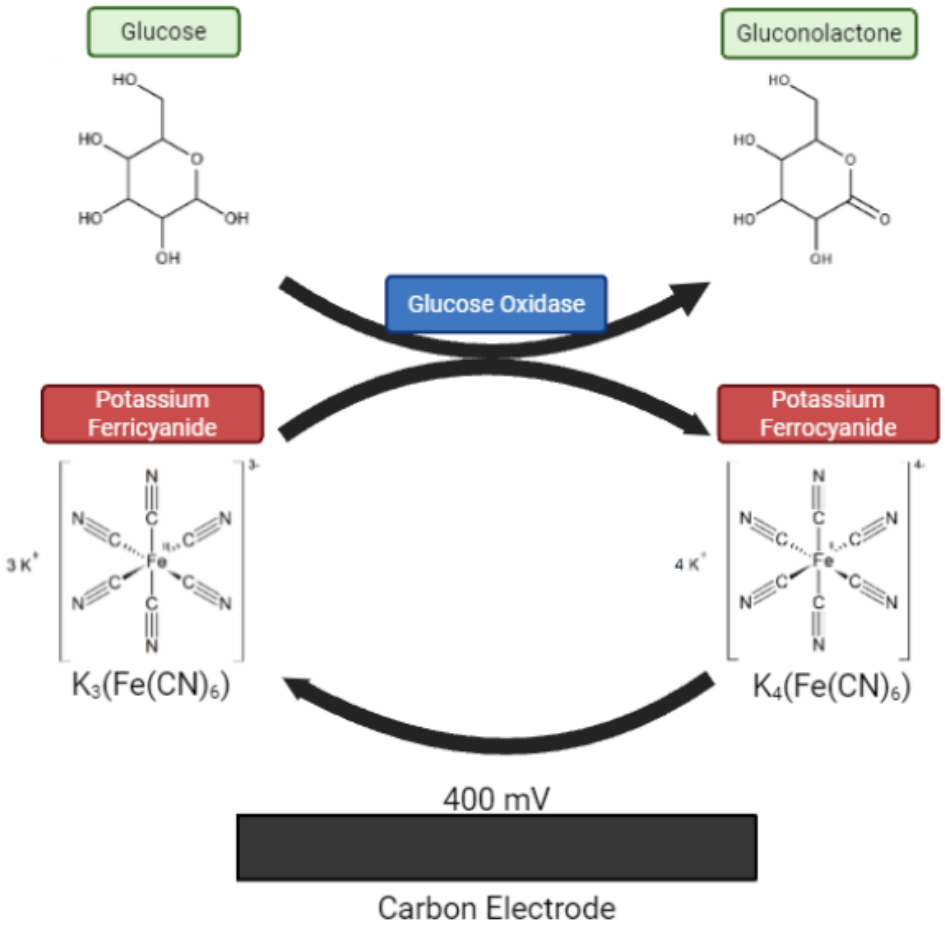

Figure 3.3: Reaction mechanism to detect glucose using the printed electrochemical biosensors with chronoamperometry. (Modified from Hassan et al. (2021))

The average current over time for various glucose concentrations is recorded for 60 seconds. The observed current at 30 seconds was used to create a calibration curve. The limit of detection was then estimated based on the standard deviation of the blank and the slope of the calibration curve (Equation 1.1.7). Using the slope of the calibration curve and electrochemically active surface area, the specific sensitivity can be calculated for each device, allowing for comparisons between them.

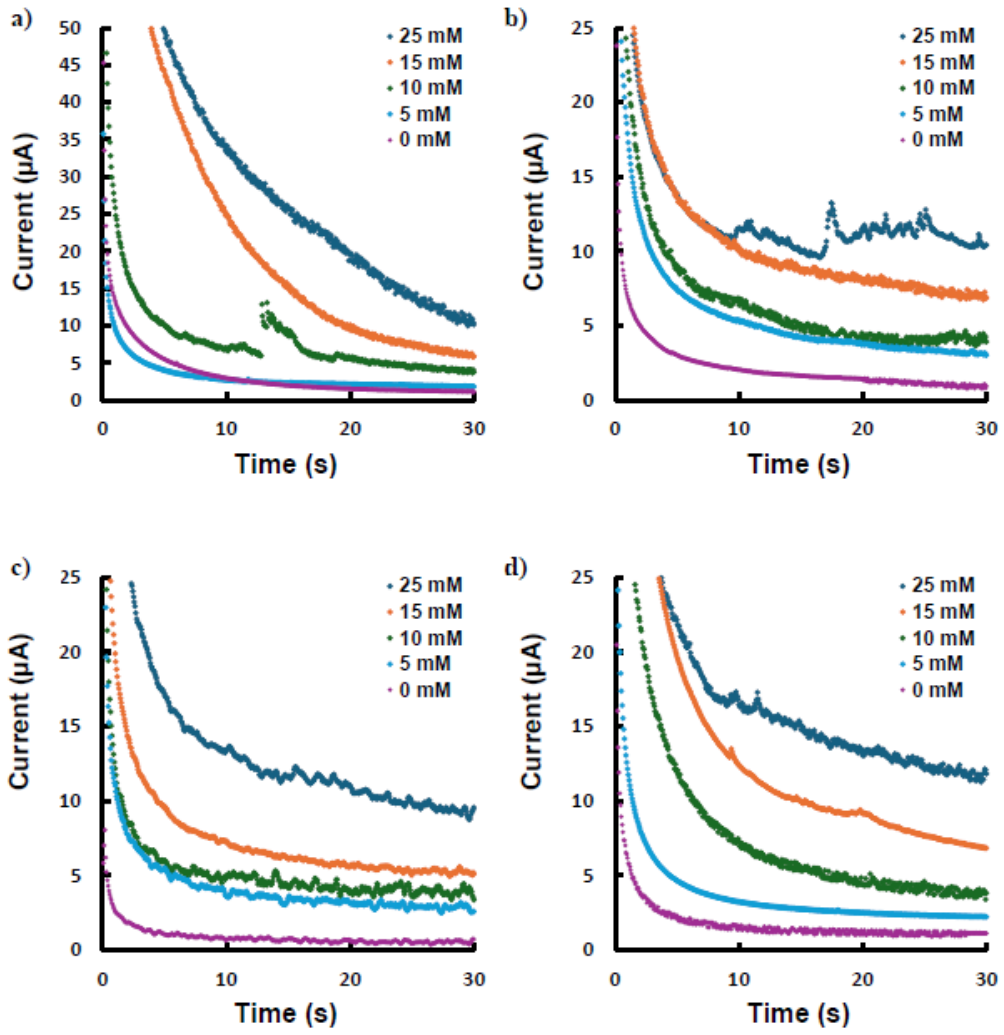
a)
b)
c)
d)
Current (μA)
Time (s)
25 mM
15 mM
10 mM
5 mM
0 mM

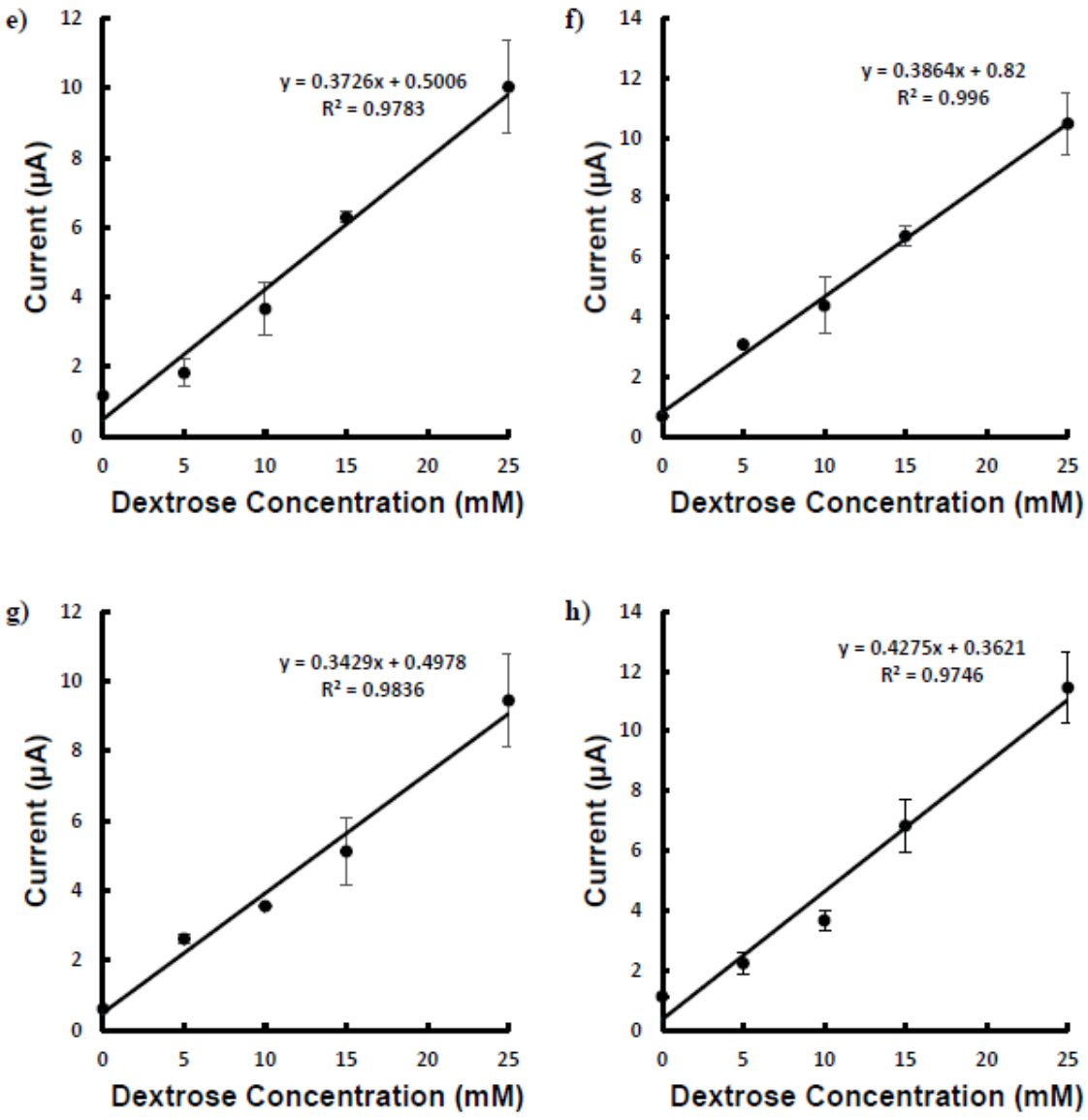

Figure 3.4: Chronoamperometric curves for glucose concentrations ranging from 0 mM to 25 mM for a) 4M4E, b) 4M2E, c) 2M4E, and d) 2M2E. Calibration curves for glucose concentration as a function of current at time = 30 seconds for e) 4M4E, f) 4M2E, g) 2M4E and h) 2M2E. The microfluidic channels were printed using materials with 8% PVA, and testing was done using PARSTAT 2263.

The calibration curve shows that the current was linearly proportional to the glucose concentration between the ranges of 0-25 mM. The linear relationship and high R-squared value prove the validity of the chronoamperometric method for the electrochemical detection of glucose. Using the calibration curve, a LOD was estimated for each printed device. The LOD for 4M4E was 0.267 mM, and 4M2E was 0.295 mM. 2M4E and 2M2E were 0.249 and 0.266 mM, respectively. This LOD value was comparable to the value of 0.21-0.35 mM of the various μPEDs reported (Dungchai et al., 2009) (Nie et al., 2010b) (Zhao et al., 2013). These μPEDs featured similar device fabrication methods where the hydrophobic channel in the paper was generated using either wax patterning or photolithography. The electrodes were all printed using screen printing, the same as our method, but each of the electrodes and microfluidic channels had a different design than ours. The LOD of the printed microfluidic device was already better than the LOD of some commercially available glucose sensors (Pullano et al., 2022). The above tests reinforce the potential of printed microfluidic devices to serve as a suitable alternative to μPEDs and can handle small sample volumes like the μPEDs (Dungchai et al., 2009) (Nie et al., 2010b). However, noise still has a noticeable impact on the current signal, as shown in the chronoamperometric curves. This can lead to similar current signals despite measuring two different glucose concentrations, for example, the 5 mM and 10 mM in Figure 3.4b) or c). With each device having similar slopes, the main difference between each device is the active working area. The 2M2E device had the highest sensitivity at 10.68 μA/(mM·cm2), compared to the other devices with only single-digit sensitivity. To increase the device's performance, higher sensitivity is desirable and ways to increase the slope were investigated.

3.2 Effect of Microfluidic Structure

The material mixture used to print the microfluidic channels consists of alumina and silica particles, PVA, and DMSO. Theoretically, when this material is printed on a surface, the PVA-DMSO solution should naturally sink through the particle-to-particle gaps due to gravity. As a result, when the DMSO evaporates, an enriched polymer layer may form on the surface, physically creating a barrier that can reduce the potential ways to access the electrode. Furthermore, PVA, as a typical polymer, can also act as an electrical insulator (Van et al., 2014). The enriched PVA layer might act as an electrical resistor between the printed electrodes and the testing solution in the channel. The effect would be detrimental to the redox reaction proposed for the electrochemical detection of glucose, which needs to happen at the surface of the electrode (Seen in Figure 3.3). The less reactions happening at the electrode means the less current signal, which directly correlates to the slope and LOD. To test this theory, the PVA concentration in the material mixture was attempted to be minimized; it was concluded that 3% PVA was the lowest level for acceptable printing performance and integrity of the printed structure. This PVA concentration is significantly lower than the 8% used in fabricating the device described previously. The figures below show the chronoamperometric measurements of the device printed with the 3% PVA concentration.

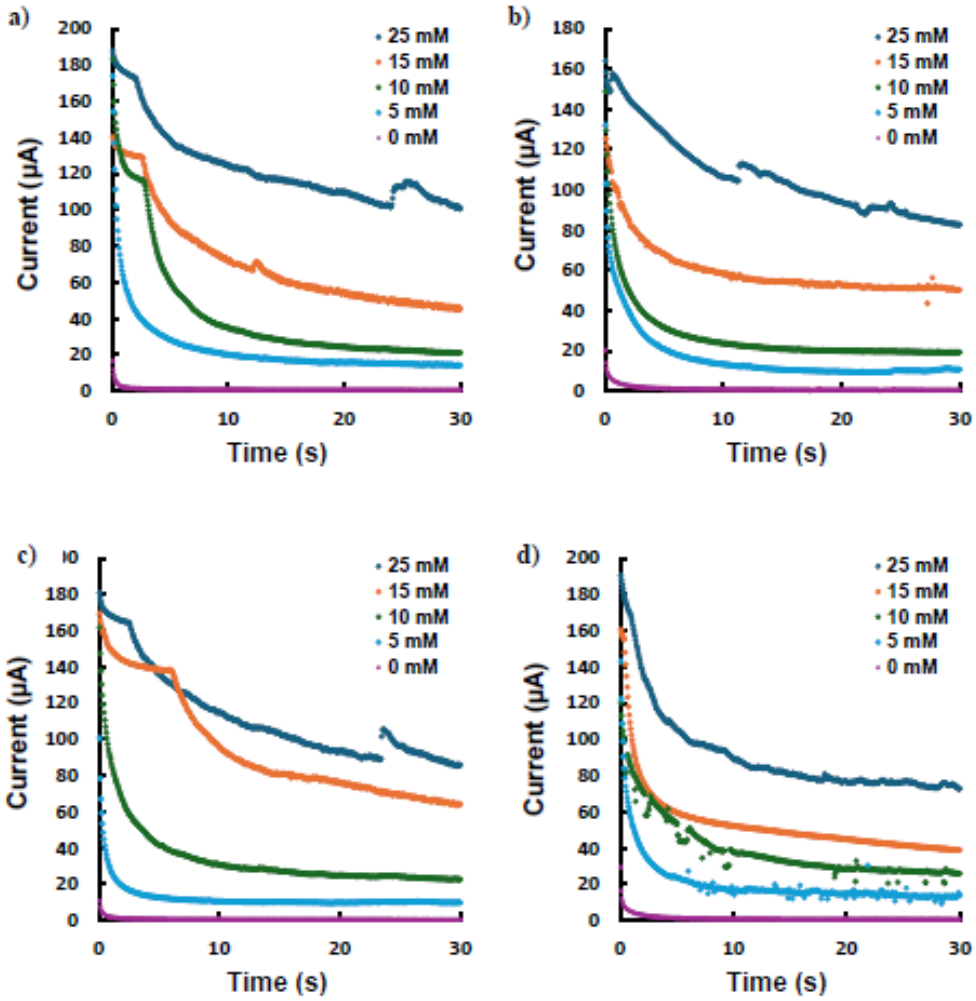
a)
b)
c)
d)
Current (μA)
Time (s)
25 mM
15 mM
10 mM
5 mM
0 mM

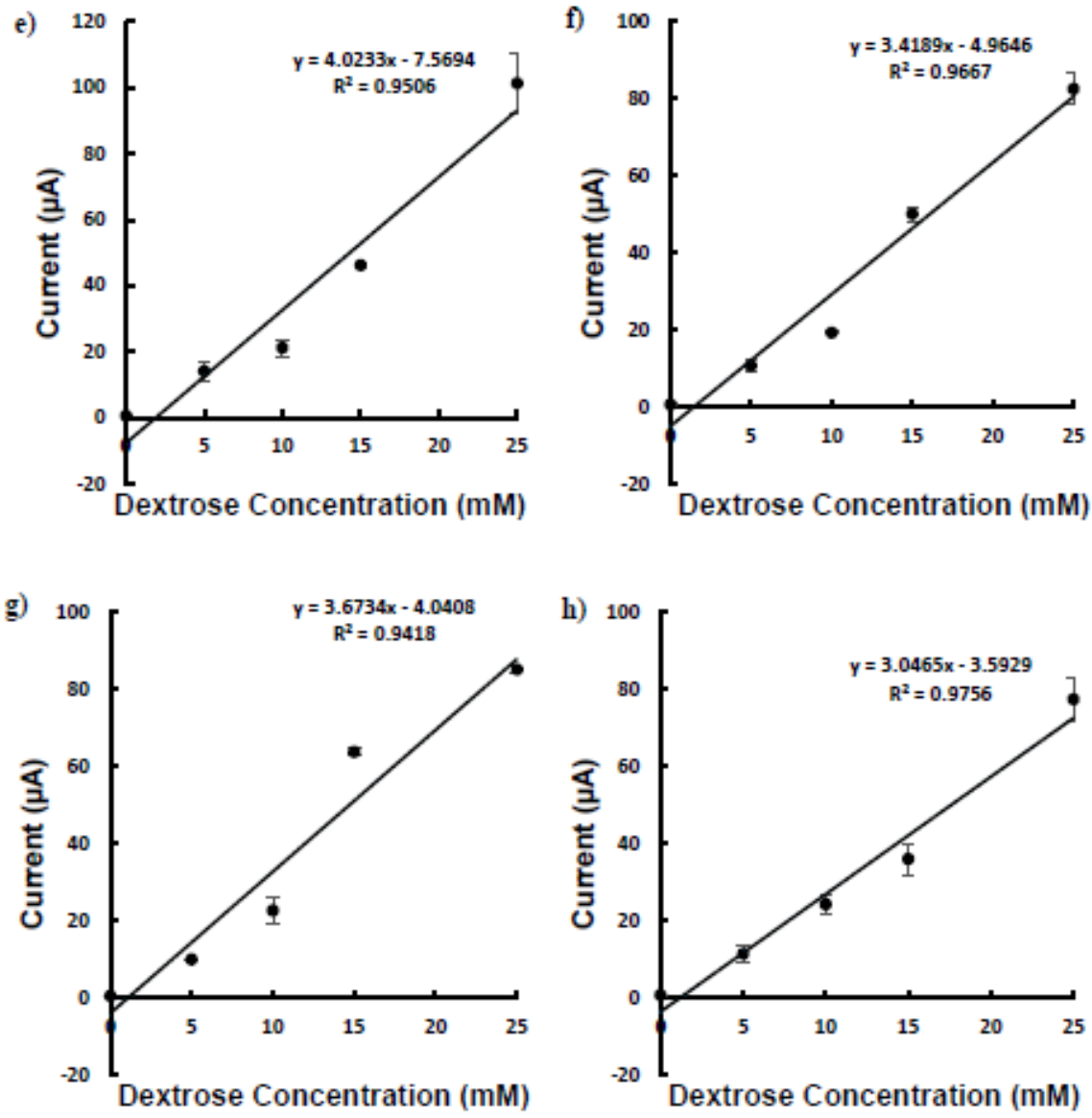

Figure 3.5: Chronoamperometric curves for glucose concentrations ranging from 0 mM to 25 mM for a) 4M4E, b) 4M2E, c) 2M4E and d) 2M2E. Calibration curves for glucose concentration as a function of current at time = 30 seconds for e) 4M4E, f) 4M2E, g) 2M4E and h) 2M2E. The microfluidic channels were printed using the materials with 8% PVA, and testing was done using PARSTAT 2263.

Looking at the chronoamperometric curves, the current signal increased with the

3% PVA material, which directly translates to a higher slope in the calibration plots. Likewise, 2M2E has the highest sensitivity at 76.1 μA/(mM·cm2). The 4M2E and 2M4E devices had a sensitivity of 42.7 and 45.9 μA/(mM·cm2), respectively. 4M4E devices had the lowest sensitivity at 23 μA/(mM·cm2). This result supports the initial hypothesis that PVA acts as an electrical insulator between the microfluidic channel and the electrode. By printing with a material that features a lower PVA %, there was less resistance to the current measured between the two electrodes, leading to a significant improvement in slope. The LOD for the various devices was calculated to be 0.066 mM, 0.128 mM, 0.068 mM, and 0.087 mM for 4M4E, 4M2E, 2M4E, and 2M2E, respectively. This is a substantial decrease compared to their 8% PVA counterparts. In terms of reported works, this LOD is comparable with more recently published μPEDs, which feature LODs of 0.06 and 0.05 mM (Li et al., 2015) (Li et al., 2016). The mentioned devices feature a fabrication process that is complicated, expensive, non-scalable and time-consuming. One device used wax-patterned hydrophilic zones and stencil printing to print the electrodes on paper. Then, the hydrothermal growth of zinc oxide nanowires on top of the working electrode totaled over eight hours to fabricate the devices (Li et al., 2015). The other sensor required baking for two hours to generate the hydrophilic zones, then manually cut and pencil-drawn electrodes (Li et al., 2016). Both devices all featured different device and electrode designs. Ultimately, the simplicity of just changing the PVA % in the material and seeing such an improvement in the result is promising.

However, printing the microfluidic channel using the 3% PVA material did have downsides; for example, the channels are less uniform in film and less scratch-resistant than the ones printed using 8% PVA. From SEM images (Figure 3.6, the microfluidic

channels printed with only 3% PVA are slightly more porous than those printed with 8% PVA; as PVA acts as the binder to hold the particles together and can fill the packing voids of the particles, the above results are expected and the natural consequence of having less PVA. Due to the poorer film uniformity, some of the edges of the channel were porous, and when the solution was dropped onto the channel for testing, the solution would spill through the channel onto the electrode, affecting the measurement, as shown in Figure 3.7. This drawback must be addressed without sacrificing the benefit of low PVA concentrations. Another outcome of the nonuniformity is the increase in standard deviation due to the devices having a more erratic structure. This is reflected in the LOD; despite the slope increasing by roughly tenfold, the LOD did not mirror the change due to the standard deviation of the blank increasing by twofold as well. Additionally, the R-squared value is also lower by approximately 2% on average compared to devices printed with 8% PVA; this could signify more randomness and variability in the data.

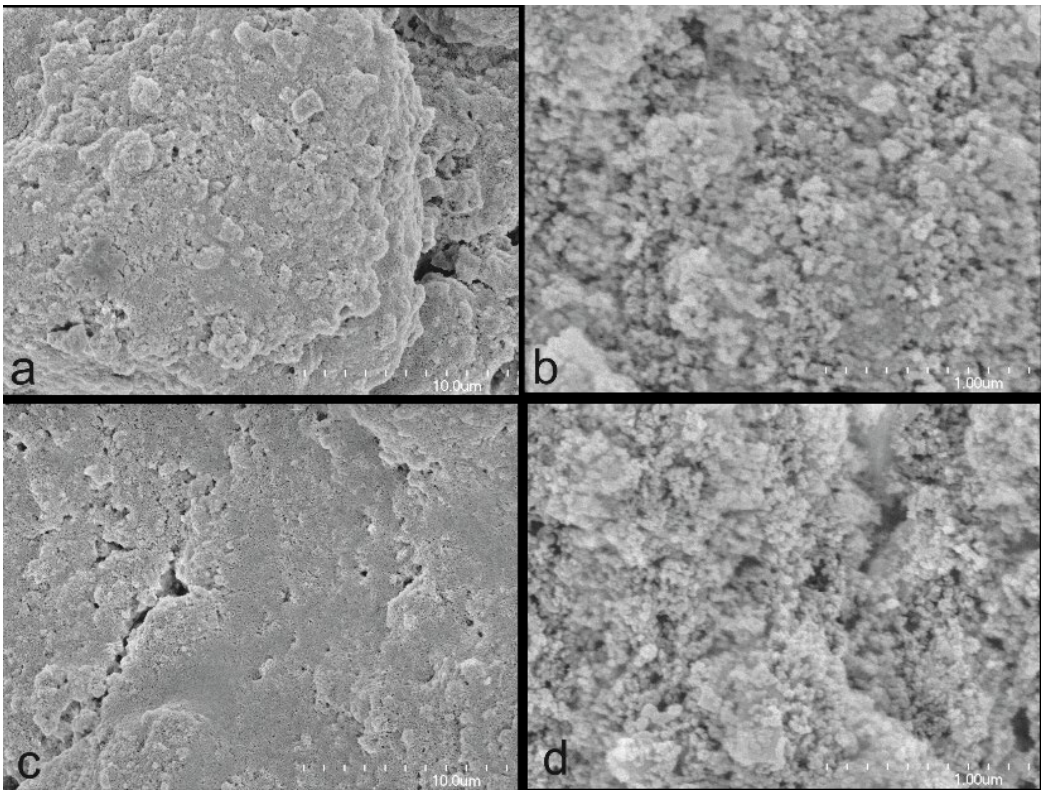

Figure 3.6: SEM images for the microfluidic channels (a, b) printed with the materials with 8% PVA and the channels (c, d) printed with the materials with 3% PVA.

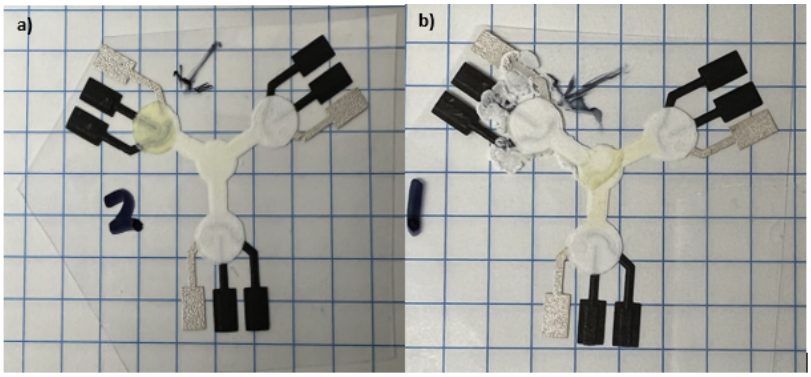

Figure 3.7: Comparison of the multichannel device after chronoamperometry experiment, a) 8% PVA and b) 3% PVA.

To overcome the above shortcomings of the devices printed with 3% PVA material,

a new microfluidic channel composition was proposed. The 3% PVA material would be printed only for the first layer, and the 8% PVA material would be printed on the second layer. This "hybrid" channel model used the higher PVA material to cover the lower PVA to improve film uniformity and scratch resistance. Chronoamperometry was conducted with hybrid microfluidic channel devices.

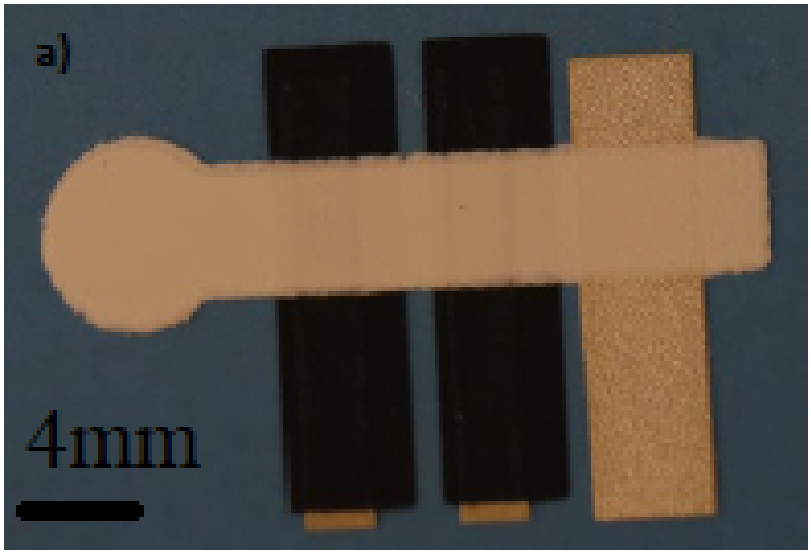

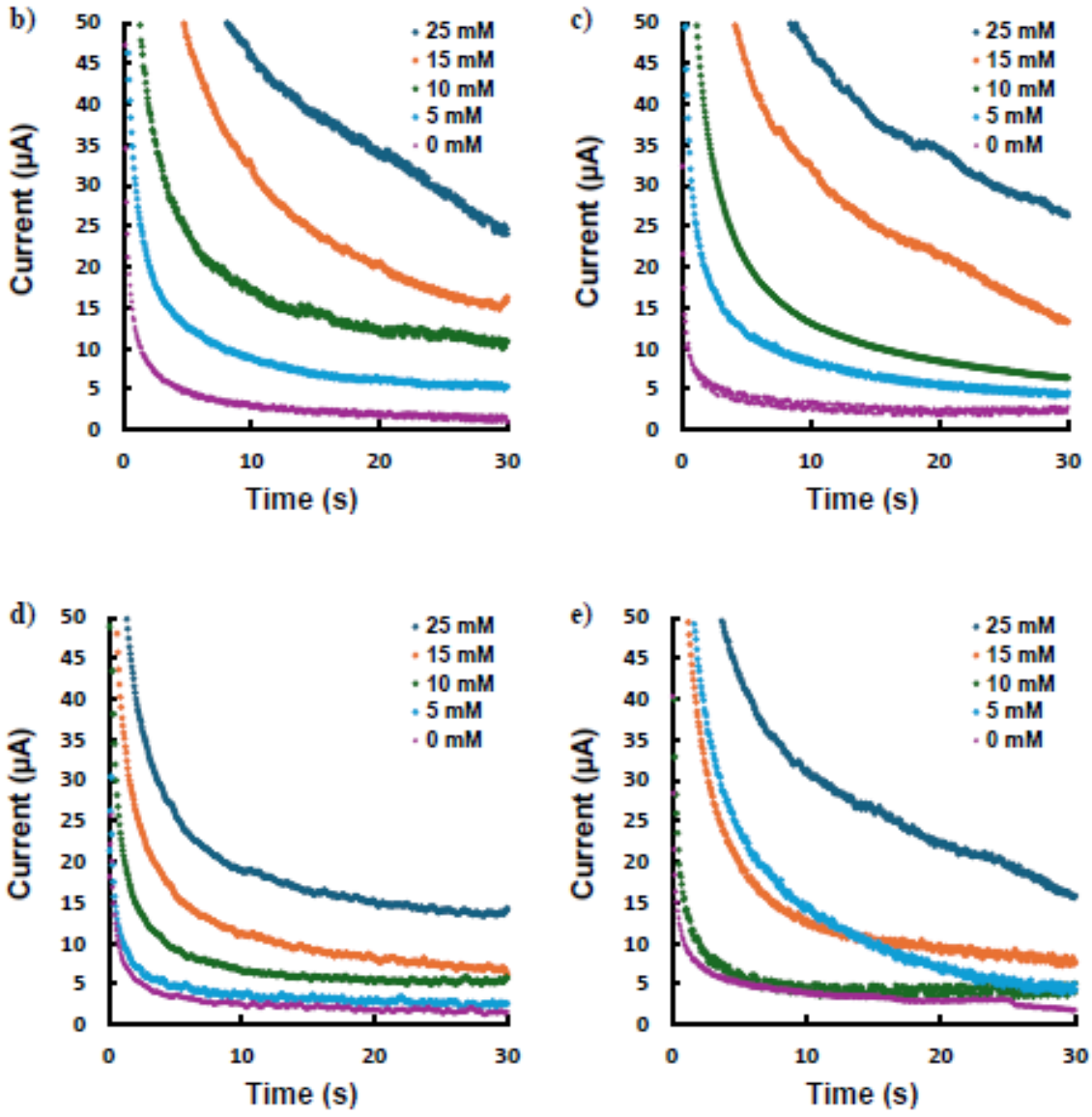
b)
c)
d)
e)
Current (μA)
Time (s)
25 mM
15 mM
10 mM
5 mM
0 mM

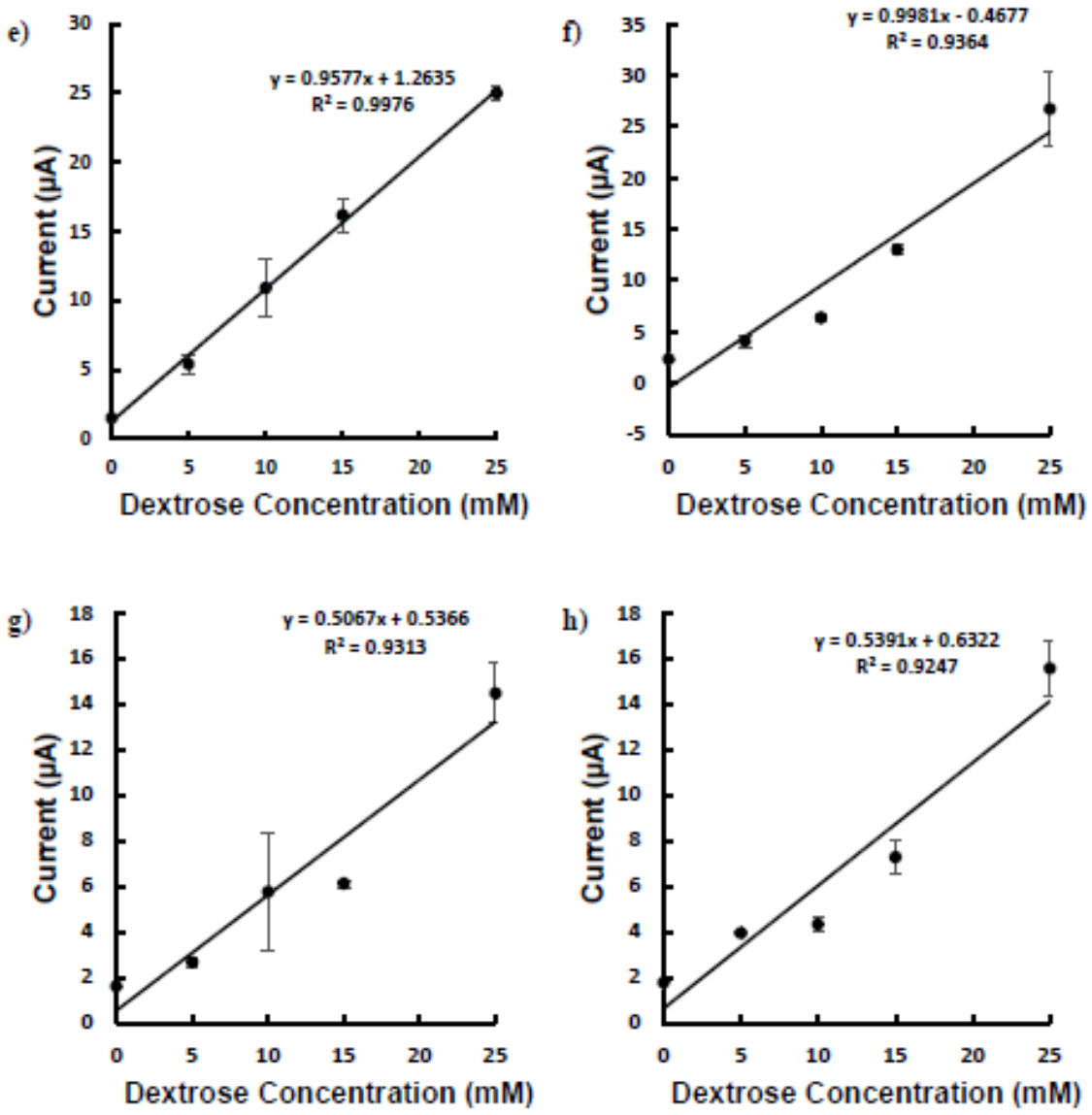

Figure 3.8: a) Picture of the 4M4E hybrid channel device. Chronoamperometric curves for glucose concentrations ranging from 0 mM to 25 mM for b) 4M4E, c) 4M2E, d) 2M4E and e) 2M2E. Calibration curves for glucose concentration as a function of current at time = 30 seconds for f) 4M4E, g) 4M2E h) 2M4E and i) 2M2E. The hybrid microfluidic channels were printed using the materials with 3% PVA as the first layer and 8% PVA on the second layer. Testing was done using PARSTAT 2263.

Looking at the calibration curves, the effect of changing from a double layered 3% PVA material to a mixed channel with 3% PVA material on the bottom and 8% PVA material on top is noticeable. The slope was reduced, but the signal from the devices differed between the 4mm and 2mm microfluidic channels. The LOD for each of the devices was all approximately 0.089 mM, with 2M4E having the lowest LOD at 0.084 mM. Although the slope of the 4mm channel devices was nearly twofold that of the 2mm channel devices. The standard deviation for the 2mm channel devices was also half that of the 4mm device, which accommodated the difference. This results in the LOD of all the devices still being within a similar range. The hybrid channel was also effective in sealing the channel and prevented any spilling of the solution during testing. Overall, it shows that the hybrid channel can overcome the shortcomings of the device printed with lower-PVA materials.

These tests highlighted the importance of controlling the standard deviation, and even with a weak current signal or sensitivity, the LOD can still be very low. An interesting observation is that the R-squared value decreased again during the hybrid channel testing, suggesting some levels of variability were not accounted for. Therefore, further testing was done using the hybrid channel model to improve the slope while maintaining the standard deviation.

3.3 Immobilization Effect

When glucose solution was dropped into the detection zone and allowed to flow through the microfluidic channel for chronoamperometry measurements. This could wash the glucose oxidase enzyme away from the working electrode, meaning that the

mediator potassium ferrocyanide must diffuse farther to be oxidized back to potassium ferricyanide. If the glucose oxidase was directly on top of the electrode, then the potassium ferrocyanide can easily diffuse just the thickness of the channel to reach the electrode. This enzyme-washing effect has been observed in previous colorimetric glucose detection in μPADs, causing uneven color change (de Freitas et al., 2018). In electrochemical detection, this washing effect would cause inconsistent measurements as the enzyme concentration was not static across all devices. Therefore, an immobilization step was added before the glucose oxidase enzyme was dropped to treat the alumina and silica particles within the microfluidic channel. Functionalizing the microparticles to hold onto the glucose oxidase. 3-aminopropyltrimethoxysilane was chosen for surface modification following the steps reported (Lee et al., 2018). Figure 10 reports the impact of immobilization on the performance of the printed hybrid channel devices.

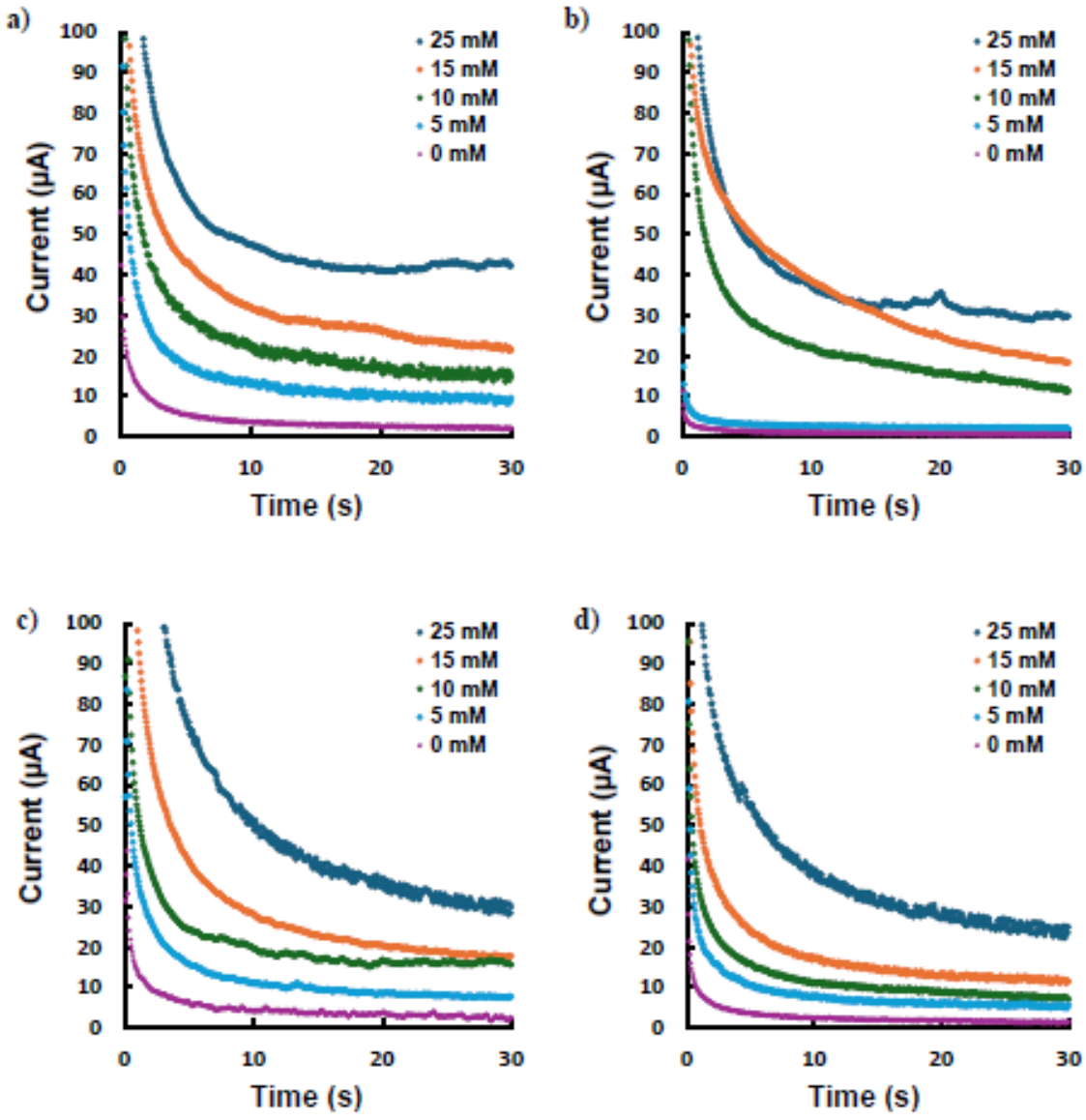
a)
b)
c)
d)
Current (μA)
Time (s)
25 mM
15 mM
10 mM
5 mM
0 mM

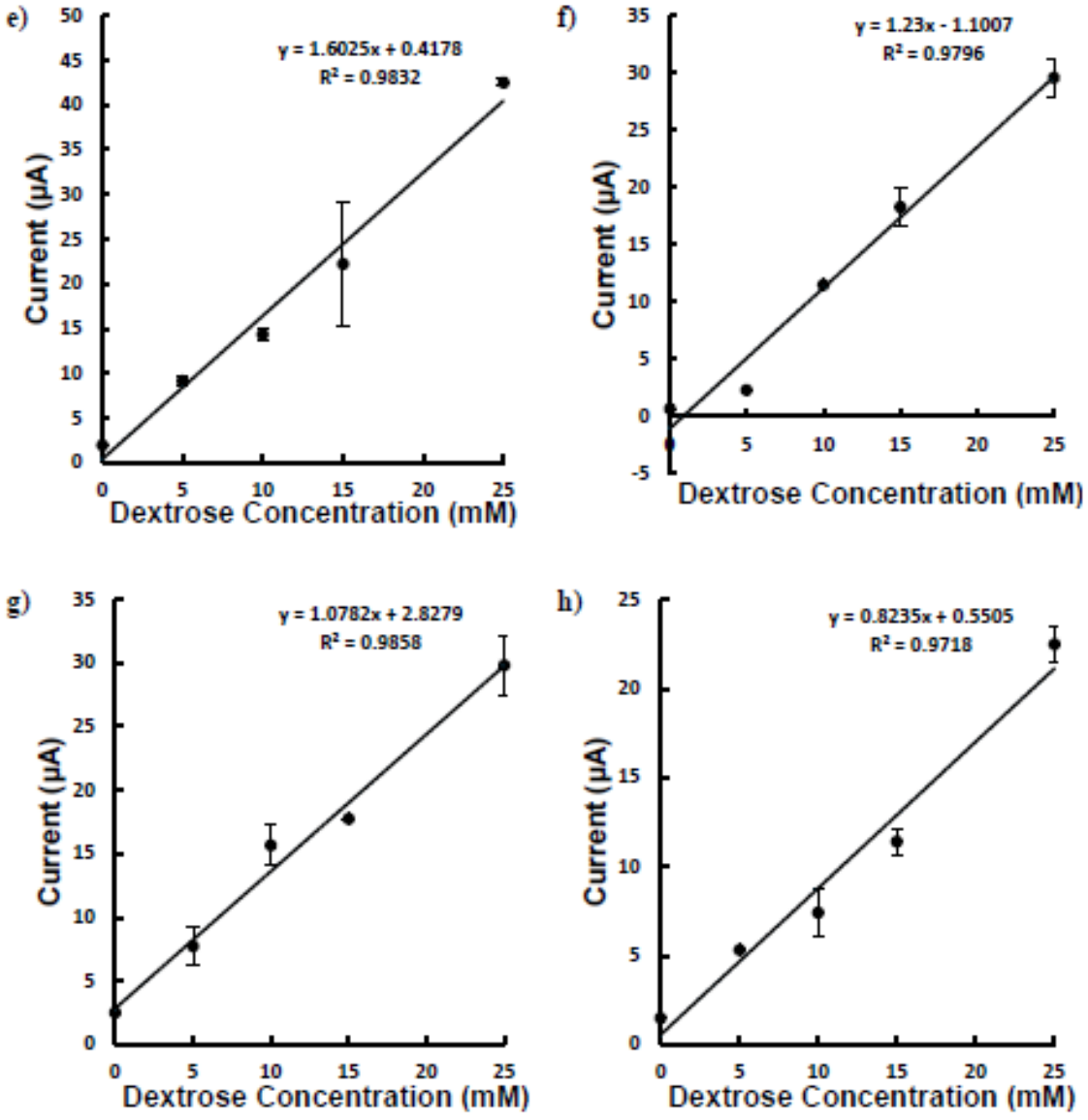

Figure 3.9: Chronoamperometric curves for glucose concentrations ranging from 0 mM to 25 mM for a) 4M4E, b) 4M2E, c) 2M4E and d) 2M2E. Calibration curves for glucose concentration as a function of current at time = 30 seconds for e) 4M4E, f) 4M2E, g) 2M4E and h) 2M2E. Retesting the hybrid channel devices with an immobilization step added before adding the glucose oxidase to the surface to modify the silica and alumina microparticles. Testing was done using PARSTAT 2263.

The LOD for all devices decreased with the addition of the immobilization step, partially due to an increase in the slope but also partly due to the lower standard deviation of the blank. The previous lowest standard deviation was ±0.013 μA for the 2M4E hybrid channel device. After the immobilization surface modification, the standard deviation was between ±0.003-0.006 μA. The lowest being 2M2E at ±0.0036 μA. As mentioned above, the LOD for the 4mm channels improved to 0.012-0.013 mM, while the 2mm channel device had worse LOD at 0.018 mM and 0.025 mM for 2M4E and 2M2E respectively. The R-squared value also increased, suggesting that the immobilization step helped remove some of the variability in prior testing. The current LOD is better, if not comparable, to the LODs of modern devices (Kant et al., 2021) (Niamsi et al., 2022). The referenced studies utilized complex surface modification or expensive gold nanoparticles to achieve such low LODs. This came at the sacrifice of ease of fabrication and cost, two pillars that made paper-based microfluidic attractive in the first place. Furthermore, the LOD achieved by the printed microfluidic device can sufficiently cover all ranges of glucose concentrations found in physiological fluids such as urine, blood, sweat, and saliva (Witkowska Nery et al., 2016). As shown by the results, the immobilization step proved beneficial and was incorporated into all subsequent experiments.

3.4 Device Features

One common difference found in the literature was often the device and electrode design as shown by the various μPEDs mentioned above (Table **??**). There is rarely a consensus on what is the most optimal device structure nor a justification for why a specific design was chosen. However, a popular electrode design is shown later. The

general principle that most designs follow is the reference electrode needs to be close to the working electrode to minimize the ohmic drop to ensure the accuracy of the measurement. In hopes of finding some guidance for novel device designs, the multi-channel devices were tested in comparison with their straight-channel counterparts to see the impact of different designs. Additionally, the reasoning behind the different results from the hybrid devices were investigated. Various experimental parameters and device features are summarized in the table below.

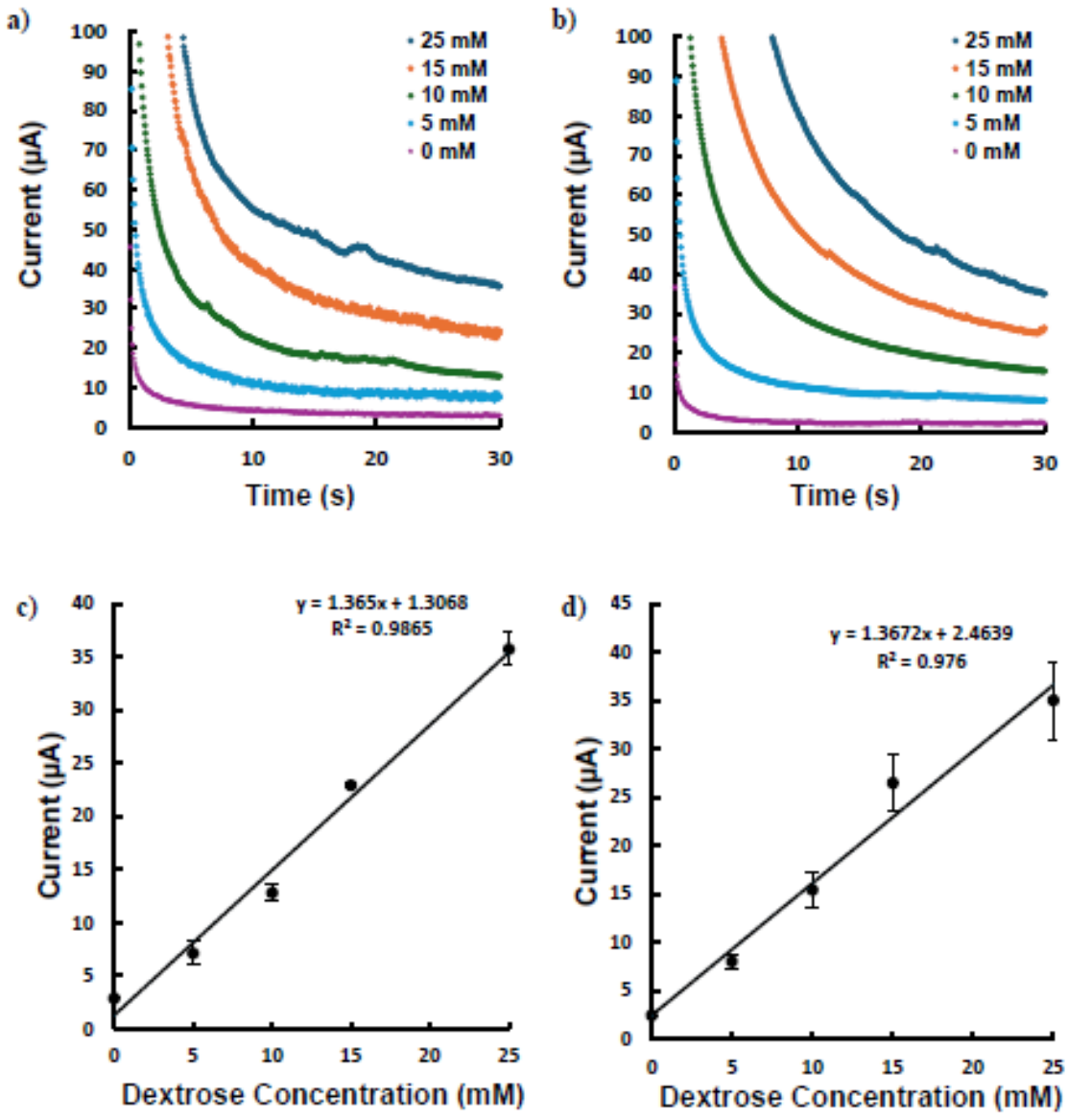

Figure 3.10: Chronoamperometric curves for glucose concentrations ranging from 0 mM to 25 mM for a) 3mm wide multichannel and b) 2mm wide multichannel. Calibration curves for glucose concentration as a function of current at time = 30 seconds for c) 3mm wide multichannel and d) 2mm wide multichannel. Testing was done using PARSTAT 2263.

Device Co-dename	Microfluidic Channel Width (mm)	Electrode Width (mm)	Electrode-Resistance (Ω)	LOD of Glucose (mM)	Sensitivity (μA/ (mM$\times$ cm^2))	Standard Deviation (μA)
Hybrid-4M4E	4	4	2.88 $\pm$ 0.19	0.01281	10.02	0.00622
Hybrid-4M2E	4	2	3.92 $\pm$ 0.24	0.01157	15.37	0.00432
Hybrid-2M4E	2	4	3.08 $\pm$ 0.12	0.01848	13.48	0.00604
Hybrid-2M2E	2	2	3.42 $\pm$ 0.25	0.02339	20.59	0.00622
Hybrid-Multi-3mm	3	1	N/A	0.01524	45.50	0.0063
Hybrid-Multi-2mm	2	1	N/A	0.014	45.57	0.0058

Table 3.1: Comparison of the performance and other physical features of different hybrid channel device designs

Looking at the table, there were no clear relationships between the parameters that can be easily distinguished. The electrode's width, which directly has an impact on the resistance of the electrode, did not have any correlation with the LOD. However, it did impact the sensitivity calculation, as the various devices were similar in

terms of slope, and the multichannel devices had the smallest electrode, which is why they had the highest sensitivity. The standard deviation was also uniform across all devices. Among all the different designs used, the devices with 4 mm channels had the lowest LOD, but only slightly better than the multichannel devices, followed by the 2mm channel devices. This table highlights the complex interactions between various parameters and the unpredictability of the outcome when changing any variable.

3.5 Experimental Conditions

Although an immobilization step was added, the washing effect was suspected to still exist. A hypothesis for why the wider channels did better than the narrow channels in Table 3.1 was due to the difference in the width of the microfluidic channel. The same volume of glucose sample was used for all testing at 6 μL. The fluid dynamics of the same solution through a 4mm channel versus a 2mm channel will naturally be different. Two solutions were trialed, one where the glucose sample volume is adjusted based on the width of the microfluidic channel. Another solution was to increase the enzyme concentration, such that the region of interest would be oversaturated with the enzyme, causing the washing effect to be minimized. The table below summarizes the LODs of various tested enzyme concentrations and glucose sample volumes. The hybrid channel 2M2E device was chosen as the primary test subject, as it had the worst LOD in prior testing.

Device Code-name	GOx Concentration (U/mL)	Glucose volume (μL)	LOD of Glucose (mM)
Hybrid-2M2E	800	6	0.02339

Hybrid-2M2E	800	4	0.01282
Hybrid-2M2E	2400	4	0.00806
Hybrid-2M2E	2400	8	0.00895
Hybrid-2M2E	2400	10	0.012
Hybrid-2M2E	4000	8	0.00824
Hybrid-2M2E	4000	10	0.00823

Table 3.2: Changes to Experimental Testing Parameters that affect LOD

The glucose sample volume was adjusted by ratio based on the difference in area between the 2mm and 4mm wide channels. Due to the thickness being the same, it was removed from the calculation. The total area of the 2mm wide channel was found to be 88 mm2, while the area of the 58 4mm channel was 126 mm^2. The specific ratio is 1:1.43; however, for simplicity, 4 μL was chosen, which would make the ratio 1:1.5. Using the reduced volume, a better LOD was obtained and comparable to the 4mm hybrid channels. Interestingly, when the enzyme concentration was increased by threefold, the LOD was further reduced to 8 μM. The increased enzyme concentration also had a buffer effect, when the glucose volume was increased to 8 μL, the LOD remained stable at approximately 9 μM. Only when the volume was increased to 10 μL did the LOD become worse and resort to the level found when 800 U/mL of GOx was used. The elevated volumes were completely handled by increasing the enzyme concentration to 4000 U/mL. By changing the enzyme concentration, the device can handle different sample volumes, contributing to the device's versatility. Overall, 8 μM was the best result and the limit of the current configuration of the microfluidic channel and experimental parameters.

3.6 Commercial Device Testing

A unique aspect of our microfluidic material compared to other μPEDs is the transferability and portability of the material. While other μPEDs are only applicable to their specific device because paper acts both as the substrate and the microfluidic channel. Our material can be freely printed on other substrates and act as a microfluidic channel. This is beneficial because it allows for easy integration with commercial devices. One example is commercially available screen-printed electrodes. Chronoamperometric testing was done on purchased screen printed carbon electrodes from MetroOhm DropSens with and without the microfluidic material printed (Paimard et al., 2023). Various studies have done similar surface modifications, however, rarely are there any baseline measurements (Anshori et al., 2021) (Rezaei et al., 2018). Therefore, in this study, the baseline LOD of glucose for the commercial device will be established and compared with the LOD using microfluidic material.

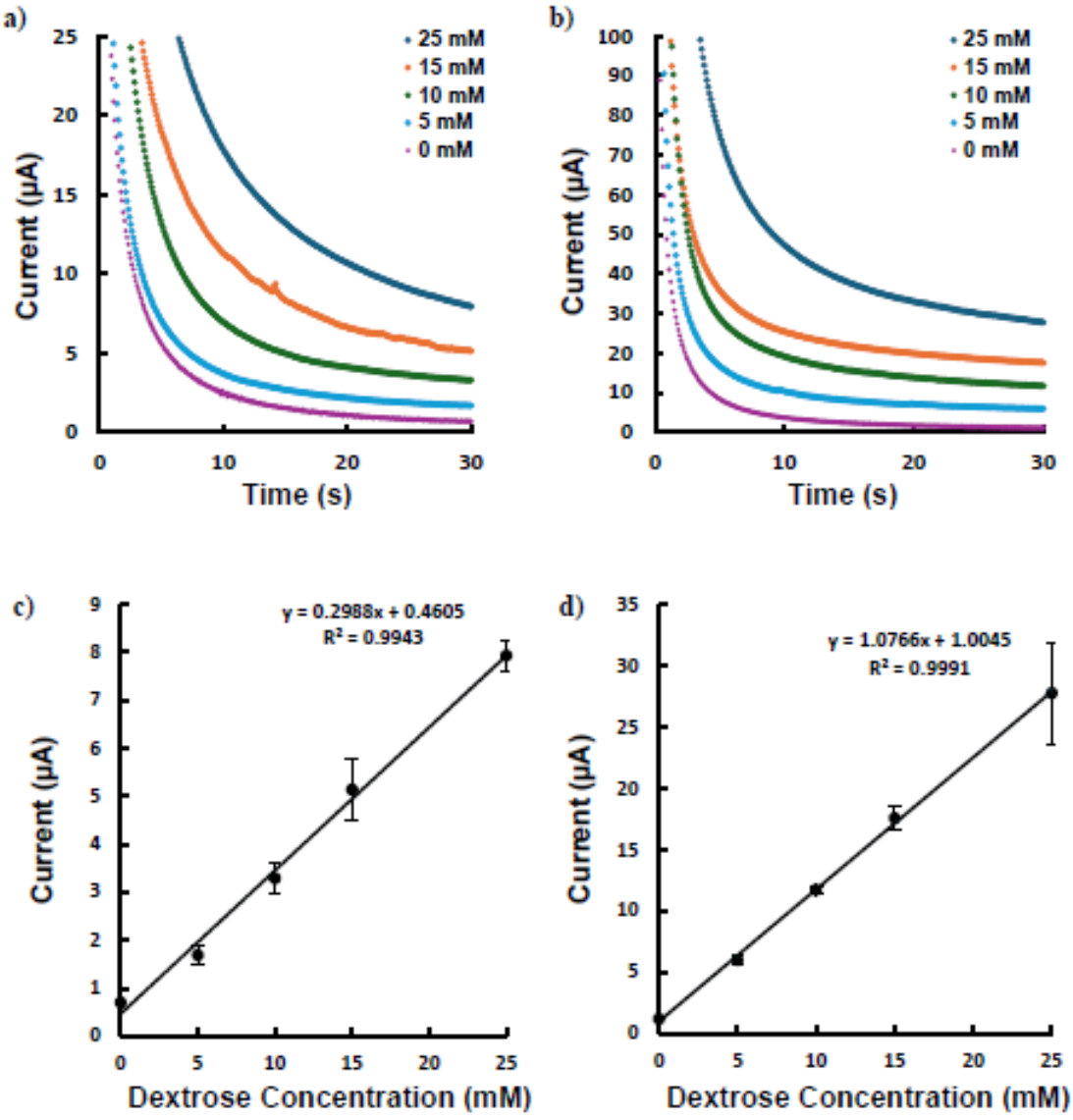

Figure 3.11: Chronoamperometric curves for glucose concentrations ranging from 0 mM to 25 mM for a) DropSens 110 and b) DropSens with 3% PVA layer. Calibration curves for glucose concentration as a function of current at time = 30 seconds for c) DropSens 110 and d) DropSens with 3% PVA layer. Testing was done using CH Instruments CHI600D electrochemical analyzer.

The LOD for the baseline commercial screen-printed electrodes was estimated to

be 0.114 mM. The device's sensitivity was calculated to be 2.5 μA/(mM $\times$ cm^2). With just one layer of the 3% PVA material, the LOD decreased to 0.023 mM with a sensitivity of approximately 9 μA/(mM $\times$ cm^2). By simply printing the microfluidic material overtop of the commercial device, it can improve the performance of the screen-printed electrodes.

Chapter 4

Results and Discussion for Semiconductive Microfluidic Channels

4.1 Semiconductive Theory

In the rapidly evolving field of microfluidics, the quest for materials that offer superior performance and functionality is paramount (Xu et al., 2016) (Kumar et al., 2019). Alumina, known for its thermal stability and chemical resistance, sees limited application in electrochemical detection due to its insulating nature (Barsoum, 2003) (Chen et al., 2021) (Novaković et al., 2021). However, as the demands for increased sensitivity, rapid response times, and enhanced electrical properties grow, the need for alternative materials becomes evident. Semi-conductive materials present a promising solution, offering unique advantages that alumina cannot provide. With their superior electrical conductivity, semi-conductive materials can significantly improve

the electrochemical performance of microfluidic devices, leading to more accurate and reliable detection of analytes (Radhakrishnan et al., 2022). In μPEDs, it has already been demonstrated the successful integration of materials such as ZnO, graphene, and similar compounds (Rezaei et al., 2018) (Charbaji et al., 2021) (Anzar et al., 2023) (Benjamin and Miranda Ribeiro Júnior, 2022). These precedents highlight the practical benefits of incorporating semi-conductive material into microfluidic devices. Moreover, transitioning from alumina to ZnO or carbon is straightforward given the current fabrication method.

4.2 Zinc Oxide Based Microfluidic Channel

The alumina can be easily substituted with ZnO during the microfluidic material formulation process. Devices printed with the ZnO microparticle as its microfluidic channel are tested using chronoamperometry.

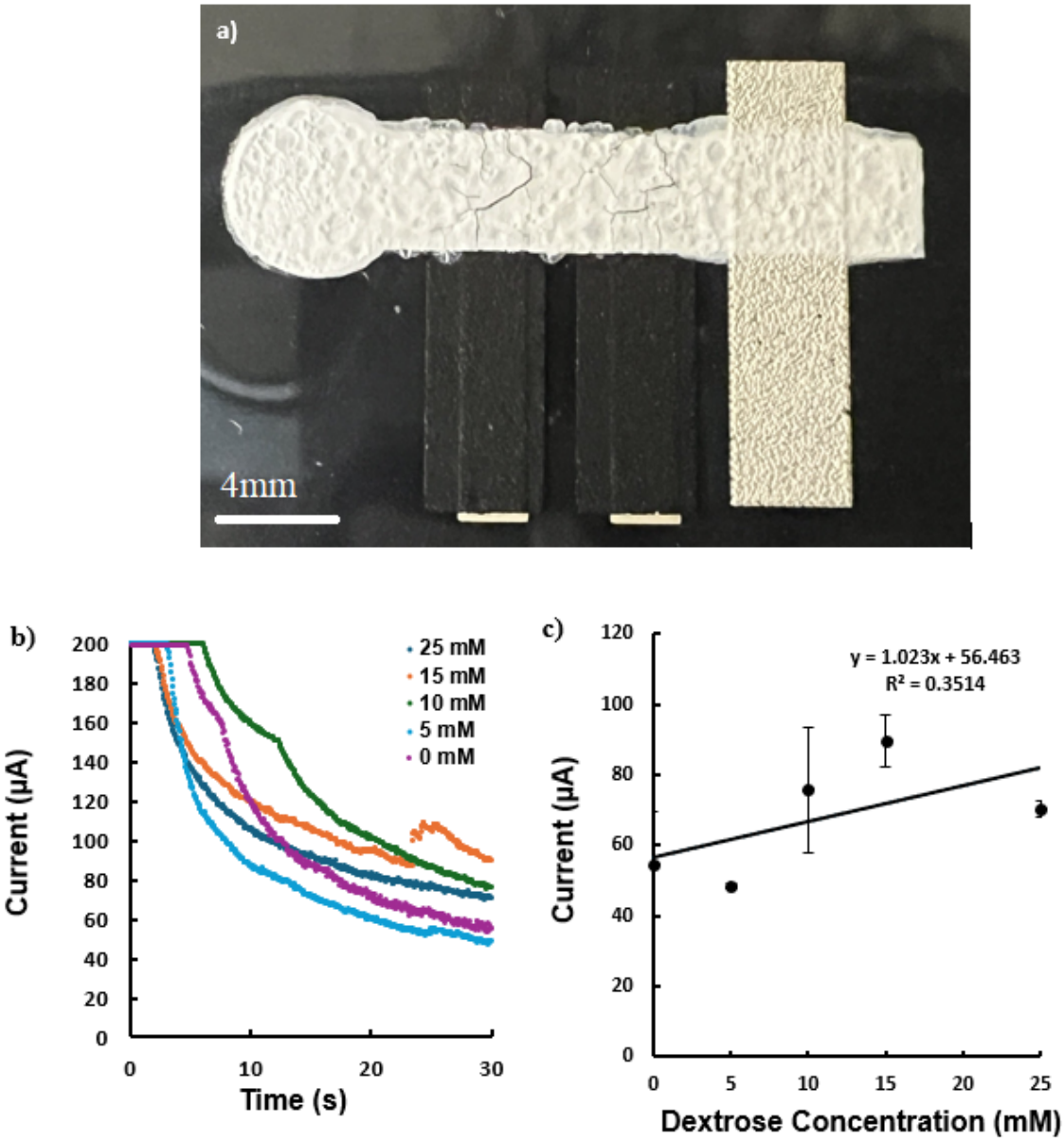

Figure 4.1: a) Picture of the 4M4E device printed with ZnO at 8% PVA with cracks over the carbon electrode. Chronoamperometric curves for glucose concentrations ranging from 0 mM to 25 mM for b) 4M4E device printed with ZnO at 8% PVA. Calibration curves for glucose concentration as a function of current at time = 30 seconds for the same c) 4M4E devices. Testing was done using PARSTAT 2263.

In the chronoamperometric curves, the initial current for each concentration started

at 200 μA for up to 6 seconds before decreasing over time. Across the various concentrations tested, the current responses were nearly indistinguishable. This was reflected in the calibration curve, where although it displayed a decreased signal with concentration, the r-squared value was significantly lower than prior tests. There was a reason to suspect that a short circuit may be occurring in the device. Typically, in a well-functioning electrochemical system, different concentrations of an analyte should result in distinct current decay profiles, as the rate of electrochemical rates varies with analyte concentration. However, in this case, the current response was almost identical regardless of the concentration. Furthermore, the changing microfluidic layer, which was composed of ZnO now instead of Al_2O_3, may have become overly conductive and had created an unintended electrical connection between the electrodes. Such a scenario would prevent the device from responding accurately to changes in analyte concentration. To test this theory, the microfluidic channel was cut in micropads, such that they were only located overtop of the electrode, acting as a surface modification to the electrode. The separated ZnO micropads were reconnected using the 8% PVA material with alumina and tested with chronoamperometry.

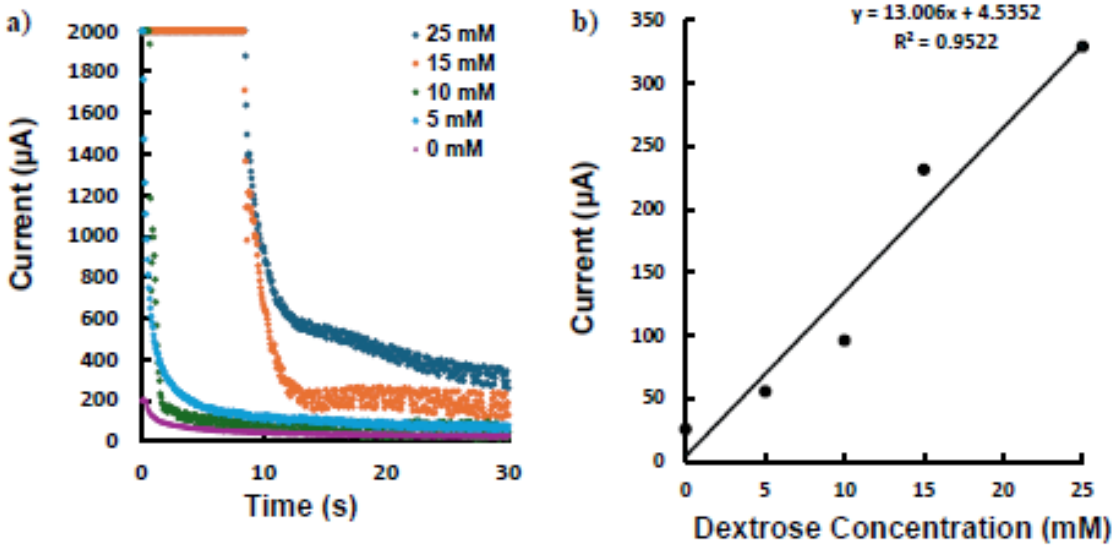

Figure 4.2: Chronoamperometric curves for glucose concentrations ranging from 0 mM to 25 mM for a) 4M4E devices with electrodes surface modified with ZnO micropads and the alumina microfluidic material printed on top. Calibration curves for glucose concentration as a function of current at time = 30 seconds for the b) 4M4E devices. Testing was done using PARSTAT 2263.

The new chronoamperometric curves show a current response over time that was more comparable to the alumina-based devices. The graphs now displayed more distinct current decay curves for the different glucose concentrations. There were still some remnants of short-circuiting. For example, for both the 25 mM and 15 mM samples, the current peaked at 2000 μA for approximately 10 seconds before decreasing. There was also a noticeable lack of filtering and an increase in signal noise. Although only one replicate was performed due to the limited number of printed devices, the results show promise, especially the slope of the calibration plot. This proved the theoretical improvements to the electrochemical performance by the introduction of semi-conductive material into the microfluidic channel to be viable. However, the method by which the semi-conductive material was introduced is critical.

4.3 Alumina with Zinc Oxide Mixed Microfluidic Channel

In hindsight, it was very optimistic to replace the alumina with ZnO and expect improvements completely. A more experimental approach was implemented, where alumina particles were partially replaced 10% at a time by ZnO. Prototyping was completed for various ratios, fluid transport, and conductivity. Given results from prior tests, the conductivity should be kept at a minimum to prevent any circuit shorting. A ratio of 80:20 and 70:30 for alumina and ZnO respectively at 8% PVA were printed and tested using chronoamperometry.

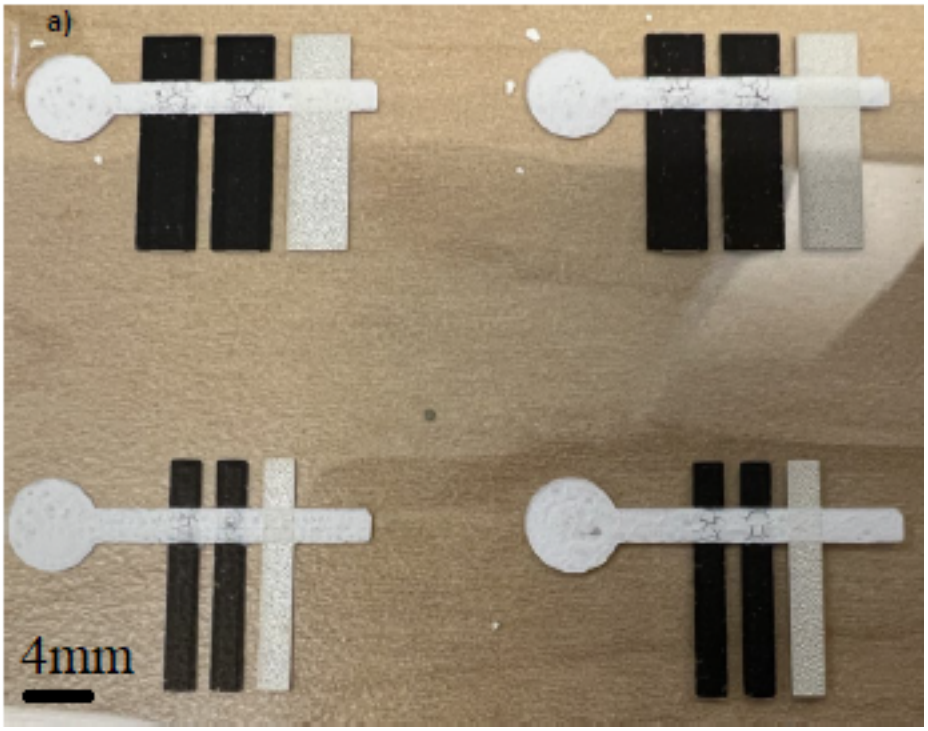

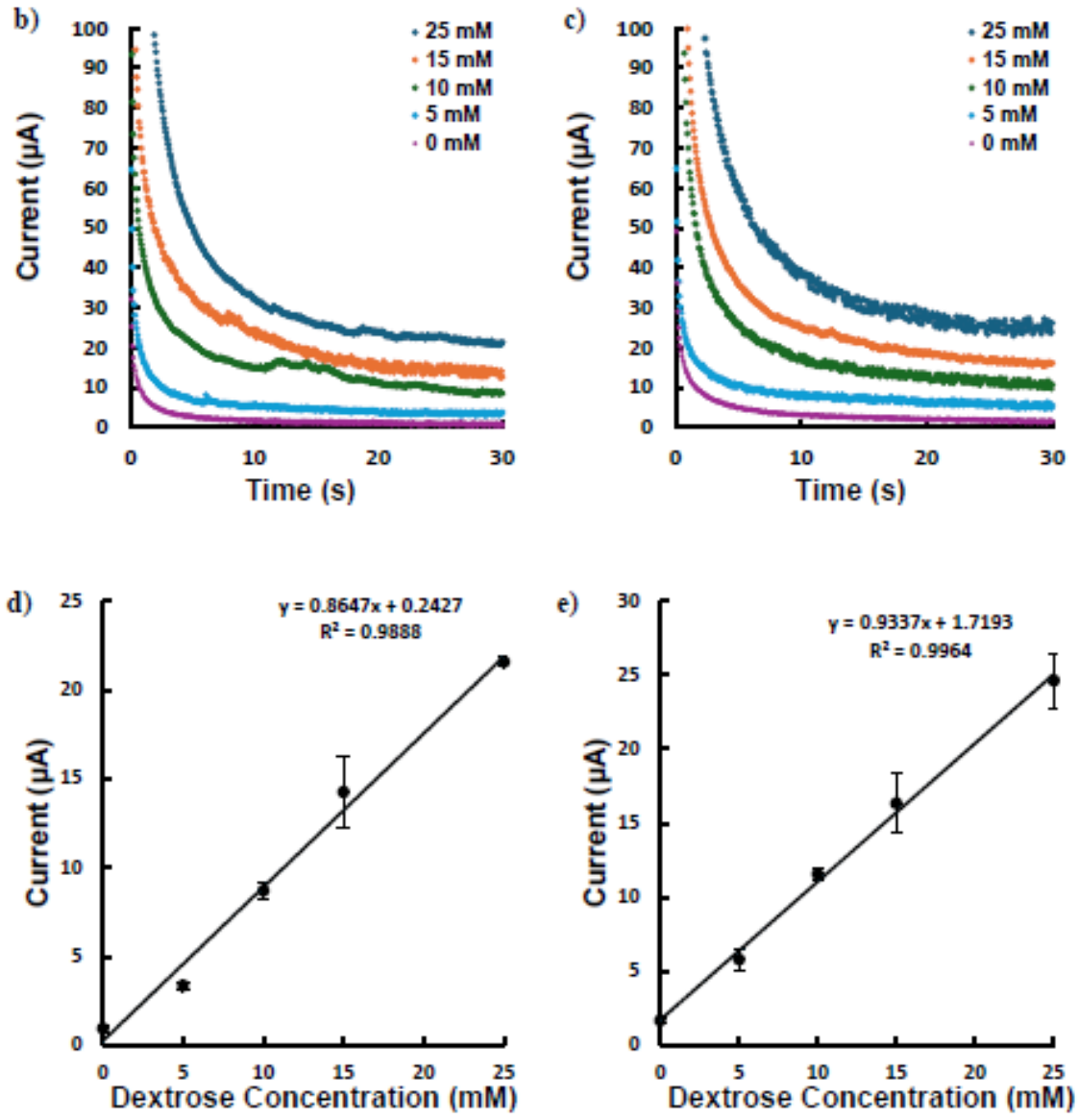

Figure 4.3: a) Pictures of the 2M4E and 2M2E devices with visible cracking over the carbon electrodes. Chronoamperometric curves for glucose concentrations ranging from 0 mM to 25 mM for b) 4M4E devices with 80:20 alumina to ZnO ratio at 8% PVA, c) 4M4E devices with 70:30 alumina to ZnO ratio at 8% PVA. Calibration curves for glucose concentration as a function of current at time = 30 seconds for the d) 80:20 4M4E devices and e) 70:30 4M4E devices. Testing was done using PARSTAT 2263.

Both compositions provided a reasonable electrochemical performance with distinct decay curves that differentiate between analyte concentrations. Just by looking at the slope, the addition of the ZnO, which was expected to improve electrochemical performance, did increase the current signal to a level comparable to that of the hybrid channels mentioned previously. However, the standard deviation was also increased, which resulted in a LOD of 0.64 and 0.52 mM for the 80:20 and the 70:30 mixed 4M4E devices, respectively. The higher standard deviation compared to when just alumina particles were used can be explained by the ZnO microparticles. The conductive nature of ZnO, combined with the fact that ZnO may not be uniformly distributed within the microfluidic layer, could lead to inconsistent electrochemical behavior. The higher ZnO also affected the structural integrity of the microfluidic channel. With the addition of ZnO, the material would often crack specifically overtop of the carbon electrodes, shown in Figure **??**A. These cracks could alter the flow of the solution or the contact between the electrodes and the microfluidic layer, introducing additional sources of variability. During this time, other solvent binder combinations and mixing methods were trialed. However, none brought significant advantages over the current method to compensate for their weaknesses. Plasma treatment was also done on the electrodes to generate a higher energy surface and allow the ZnO material to spread more easily. While plasma-treated electrodes did see better print quality and electrochemical performance, the variability between treatments made them unfavorable. Therefore, an alternative approach to integrating ZnO was tested.

4.4 Carbon Black Mixed Microfluidic Channel

Given the extensive evidence of carbon-related compounds being integrated into PEDs. A similar experiment to ZnO was conducted for carbon black. Various studies focused on carbon nanotubes or reduced graphene oxide, requiring complicated fabrication or a specific setup. Our experiment just simply used commercially bought carbon black microparticles. An additional 5% of carbon black was added to the 8% PVA material and printed. The 4M4E device was tested using chronoamperometry

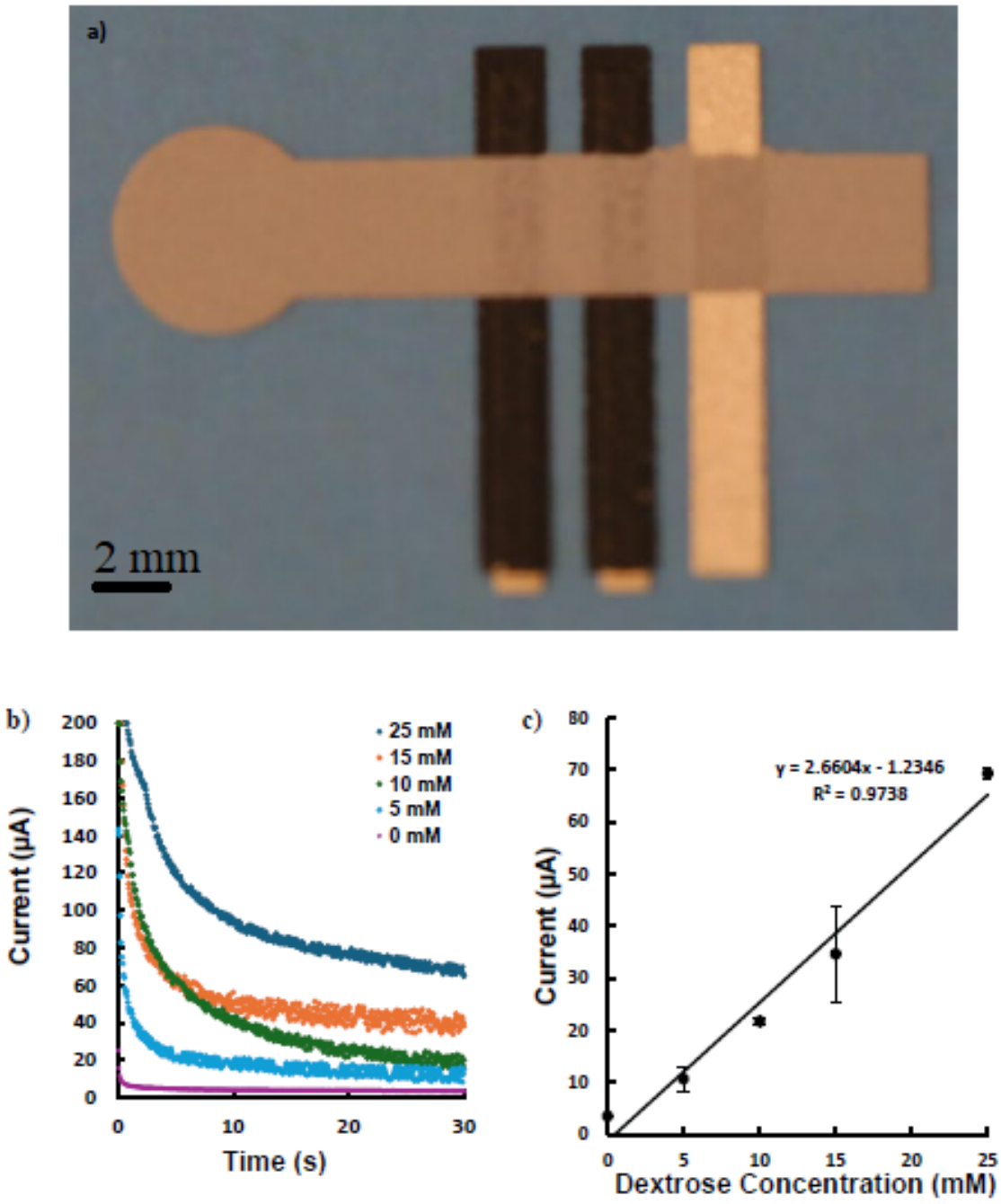

Figure 4.4: a) Picture of the 4M2E device printed with alumina mixed with carbon. Chronoamperometric curves for glucose concentrations ranging from 0 mM to 25 mM for a) 4M4E devices with alumina mixed with 5% carbon black at 8% PVA. Calibration curves for glucose concentration as a function of current at time = 30 seconds for the same b) 4M4E devices. Testing was done using PARSTAT 2263.

While the main purpose of the ZnO microparticles was to increase the conductivity of the channel to allow for easier current measurement. The carbon microparticle has an additional role. Carbon black has a high surface area; when dispersed within the alumina matrix, it could potentially increase the effective surface area of the electrode, providing more active sites for electron transfer. This is crucial in chronoamperometry, as it improves the sensitivity and allows for more efficient detection of analytes in theory. The chronoamperometry curves and calibration plot exhibit a higher current response when the channel contains carbon black than the pure alumina channel. A similar noise level to the ZnO mixed with alumina channels was observed, posing the same potential microparticle uniformity issue. The LOD for the alumina channel mixed with carbon black was determined to be 0.091 mM. This result confirms the incorporation of carbon black into the alumina matrix can enhance the performance of the microfluidic channel for chronoamperometric measurement but suffer from the same noise effect as mixing alumina with ZnO.

4.5 Micropad Printing on Straight Channel Design

The successful instance of ZnO measurement was done when the ZnO material was solely over top of the electrode and the microfluidic channel was manually printed using the alumina particle material. In this case, the printed ZnO acted as a surface modification to the carbon electrodes, and there were no ZnO microparticles located elsewhere in the channel that would generate noise. In the previous section, the potential of using ZnO and carbon black to enhance electrochemical properties

of these printed devices were recognized. While these modifications offered improvements, issues such as noise and inconsistent structural integrity remained prevalent. To address these challenges, this section focuses on an alternate integration method in the form of micropad printing. In micropad printing, the material will specifically be printed overtop of the carbon electrodes creating localized areas of enhanced conductivity, while maintaining overall channel stability. This approach attempts to recreate the success of the reconstructed ZnO channel measurement from the earlier section. The first micropads printed was ZnO based on the 3% PVA formula, with two layers of alumina in 8% PVA overtop as the microfluidic channel.

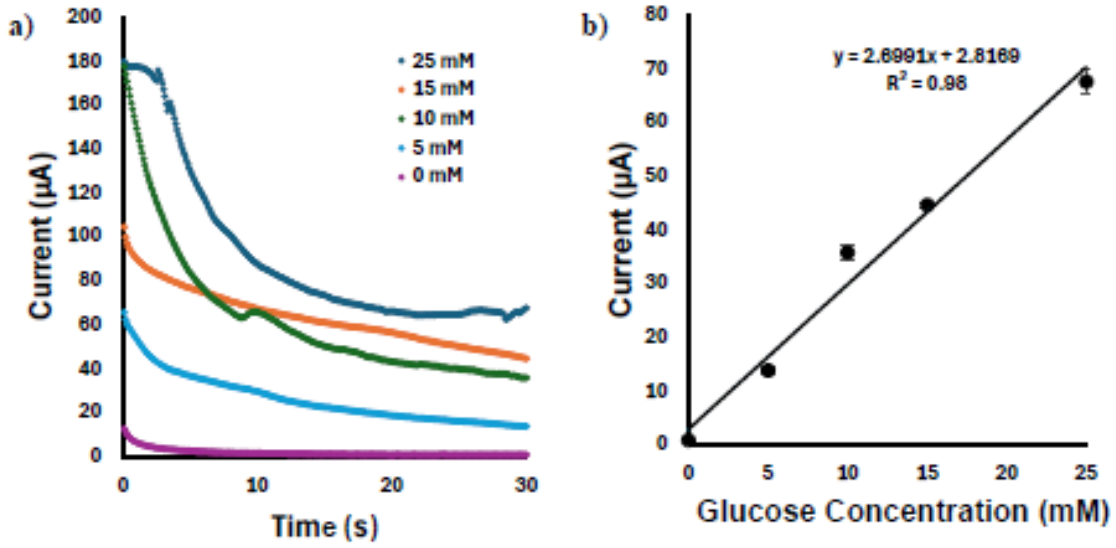

Figure 4.5: Chronoamperometric curves for glucose concentrations ranging from 0 mM to 25 mM for a) 4M4E devices with ZnO micropads based on 3% PVA formulation. Calibration curves for glucose concentration as a function of current at time = 30 seconds for the same b) 4M4E devices. Testing was done using CH Instruments CHI600D electrochemical analyzer.

The presented chronoamperometric curves depicted a regular current decay over time relationship. The signal was distinct across the various glucose concentrations,

with some abnormalities, such as the curves for 25 mM and 10 mM peaked at uniquely higher current signals and took longer to reach a steady state. Ultimately, the calibration plot saw an improvement in slope and, likewise, the LOD. The LOD for this configuration was determined to be 0.028 mM. Compared to the LOD of devices printed with just alumina material in 8% PVA, this result did improve. The signal noise was also noticeably reduced, which was likely due to the usage of a more modern and accurate electrochemical analyzer. Going forward, this new machine was used to carry out all electrochemical experiments. The ZnO micropads were still cracking, and fumed silica was a primary suspect. The ZnO material was remade without any fumed silica, and the amount of solvent was adjusted for adequate viscosity to print. The binder solvent of PVAc/DIP was also trialed without fumed silica.

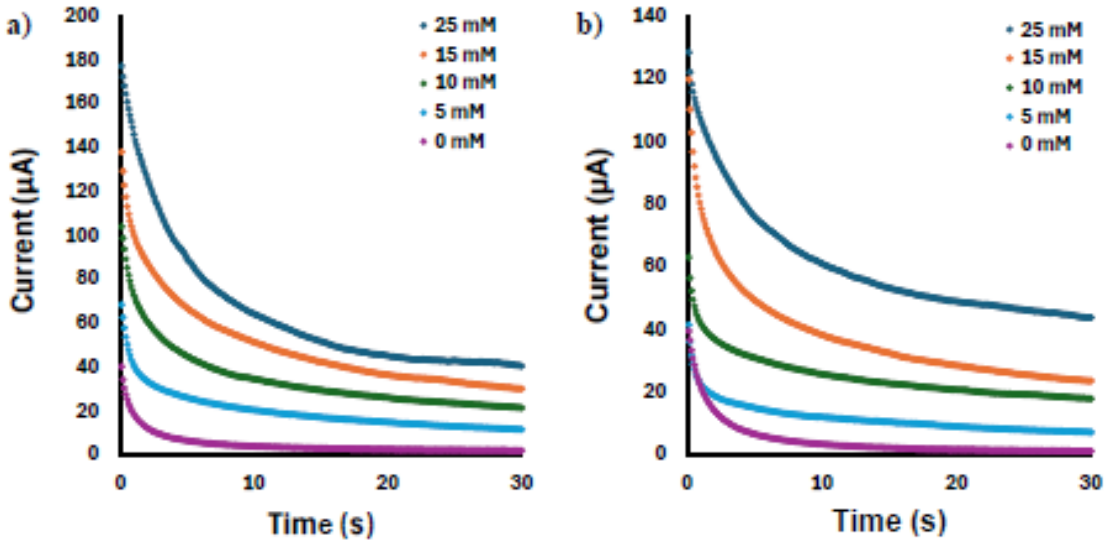

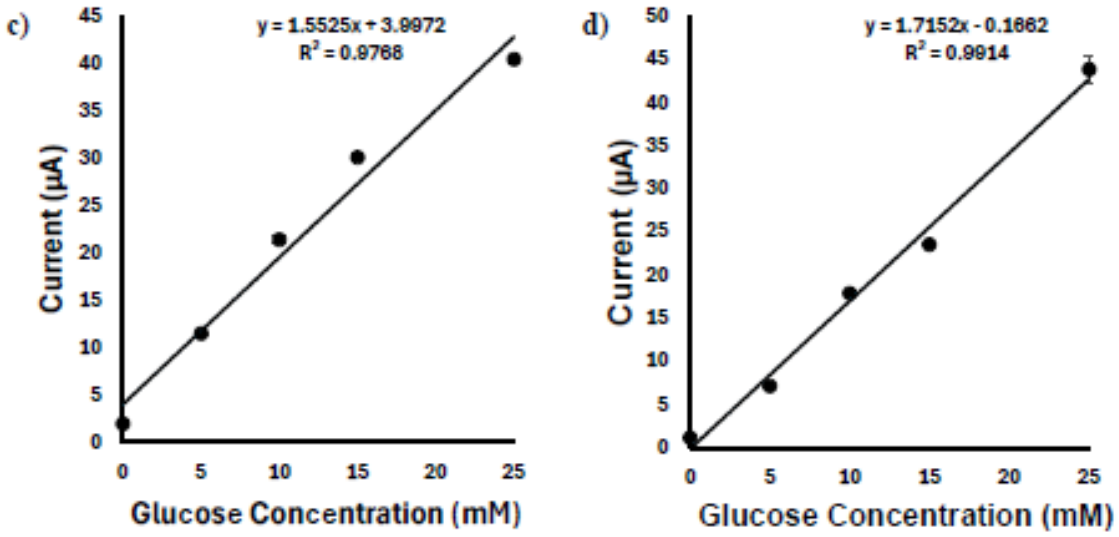

Figure 4.6: Chronoamperometric curves for glucose concentrations ranging from 0 mM to 25 mM for a) 4M4E devices with ZnO micropads based on 8% PVA formulation without the fumed silica and b) 4M4E devices with ZnO micropads with 8% PVAc/DIP without the fumed silica. Calibration curves for glucose concentration as a function of current at time = 30 seconds for the same 4M4E devices without fumed silica but with c) ZnO micropads with PVA/DMSO and d) ZnO micropads with PVAc/DIP. Testing was done using CH Instruments CHI600D electrochemical analyzer.

In the first set of graphs, the current response decreases over time, with a clear distinction between each glucose concentration. The clarity of the signal and the linear relationship in the calibration curve with a high R-square value, suggest a good validity to the result. The LOD for the devices with ZnO micropads in PVA/DMSO but without the fumed silica was 0.17 mM. However, the LOD for the device with ZnO micropads without fumed silica but made with PVAc/DIP was 0.087 mM. The removal of fumed silica from the material can decrease the signal due to several key factors related to the role fumed silica plays in the composite. The fumed silica has a high surface area and can contribute to better material dispersion within the

matrix. When fumed silica is removed, the overall amount of interconnected network within the matrix, which facilitates better analyte and mediator flow is reduced. This reduction can impact the current response, leading to a decreased signal. To remedy this problem, the same material was made except ZnO nanoparticles were used in place of fumed silica in the same amount.

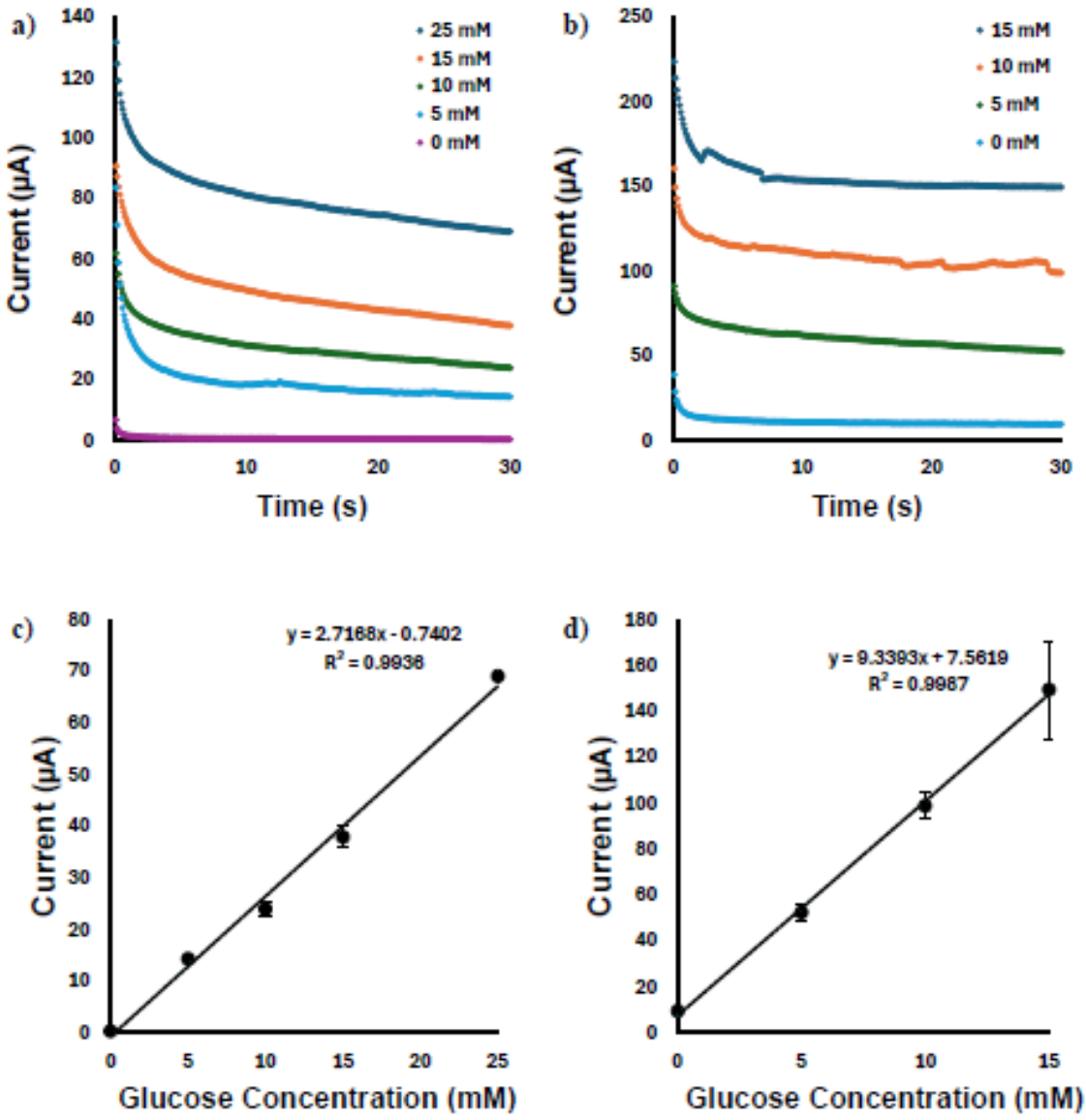

Figure 4.7: Chronoamperometric curves for glucose concentrations ranging from 0 mM to 25 mM for a) 4M4E devices with ZnO micropads based on 8 PVA formulation with ZnO nanoparticles replacing the fumed silica and b) 4M4E devices with ZnO micropads with 8 PVAc/DIP and ZnO nanoparticles in place of the fumed silica. Calibration curves for glucose concentration as a function of current at time = 30 seconds for the same 4M4E devices with ZnO nanoparticles but with c) ZnO micropads with PVA/DMSO and d) ZnO micropads with PVAc/DIP. Testing was done using CH Instruments CHI600D electrochemical analyzer.

With the addition of another ingredient, there was an increased likelihood that the material was not uniformly mixed. This was quickly noticed in the amperometric curves, where the curves appeared jagged rather than smooth. The ZnO nanoparticles did improve the signal measurement, with the ZnO micropads made with PVAc/DIP significantly increasing. The LOD for the devices with PVA/DMSO-based ZnO micropads was 0.072 mM. The devices with ZnO micropads made with PVAc/DIP had a lower LOD at 0.047 mM. This was very interesting because the PVAc/DIP combination results were very different based on which microparticle was used. When the PVAc/DIP combination was tested in alumina particle-based materials, the material was too hydrophobic to even let the solution flow. However, with a ZnO particle-based material, the PVAc/DIP combination was perfectly fit for use.

Following the steps of ZnO micropads, carbon black micropads were implemented by adding various concentrations of carbon black to the ZnO material made with 3% PVA. The same alumina material was printed overtop as the microfluidic channel, and testing was done with chronoamperometry.

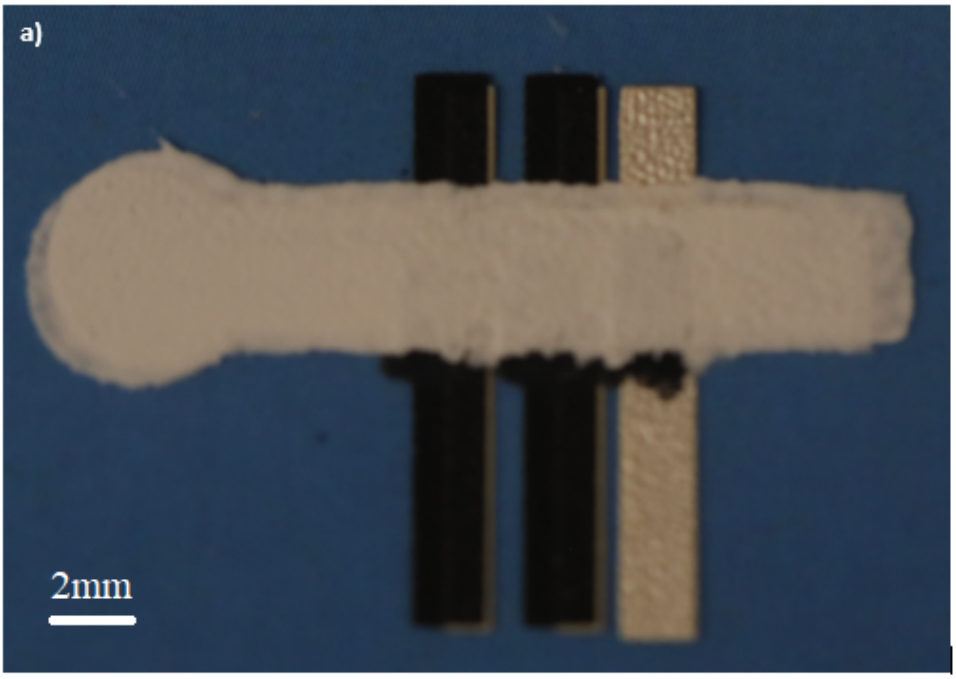
a)
2mm

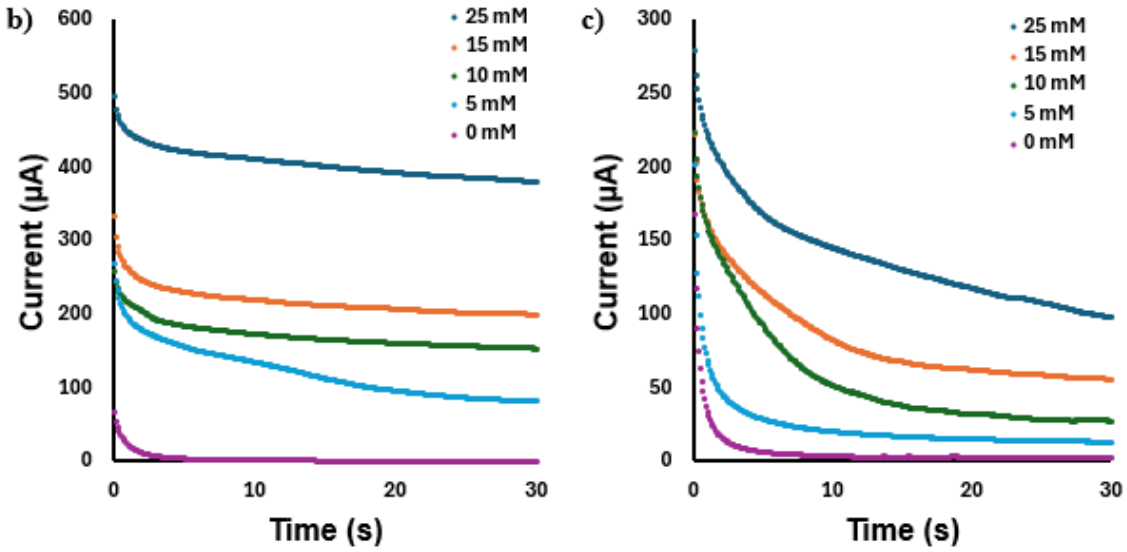
b)
Current (μA)
Time (s)
25 mM
15 mM
10 mM
5 mM
0 mM
c)
Current (μA)
Time (s)
25 mM
15 mM
10 mM
5 mM
0 mM

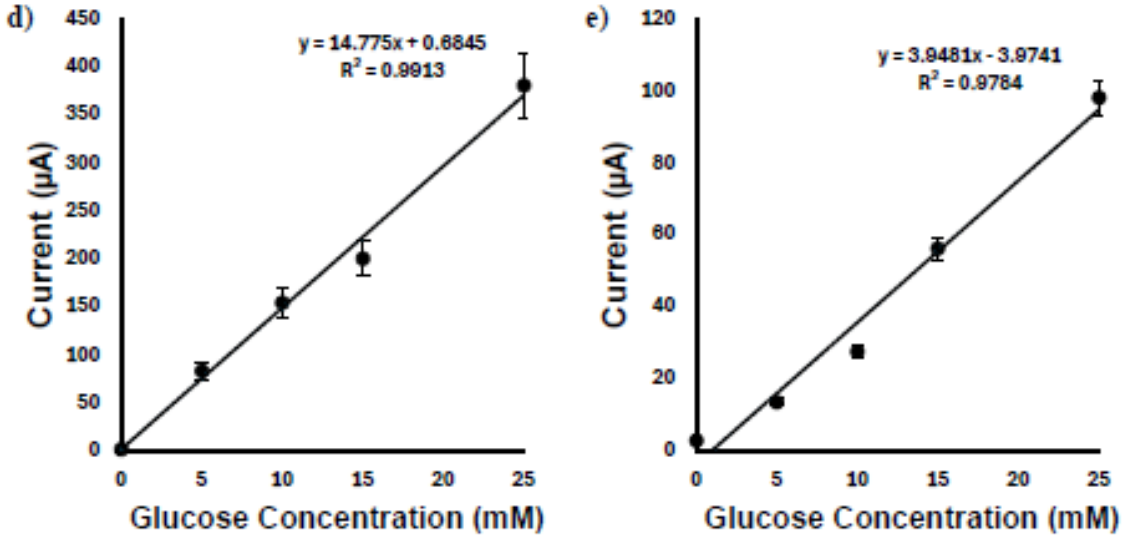

Figure 4.8: Picture of the 4M2E device with carbon black micropads. Chronoamperometric curves for glucose concentrations ranging from 0 mM to 25 mM for b) 4M4E devices with 8% carbon black micropads based on 3% PVA ZnO formulation c) 4M4E devices with 10% carbon black micropads based on 3% PVA ZnO formulation. Calibration curves for glucose concentration as a function of current at time = 30 seconds for the same 4M4E devices with d) 8% carbon black micropads and e) 10% carbon black micropads. Testing was done using CH Instruments CHI600D electrochemical analyzer.

In both micropad scenarios, the synergistic effects of having both carbon black and ZnO in the micropad are recognized. The 8% carbon black micropad saw a significant increase in current signal, matching the high slope of the reconstructed ZnO channel. The LOD for the devices with 8% carbon black micropads was estimated at 0.015 mM. The 10% carbon black micropad devices performed worse in comparison, with an LOD of 0.062 mM. The increase in sensitivity through the introduction of carbon black seemed to hit its peak at 8%, and any additional carbon black had diminishing returns. This can be explained by the carbon black particles that form aggregates. Depending on the concentration, carbon particles can agglomerate when

in excess due to Van der Waals forces and through hydrophobic interactions. This could lead to the formation of larger clusters of carbon rather than a well-dispersed distribution of particles. When used sparingly, the carbon particle can act as an electrode extension, increasing the electroactive surface area. However, when used in excess, the aggregation of carbon particles can block access to the electrode, which is critical for the redox reaction that occurs during chronoamperometry.

Another issue that persisted throughout the semi-conductive material testing was the elevated standard deviation. Despite the usage of the immobilization step and the increase in conductivity through the integration of semi-conductive particles, the standard deviation was consistently higher than testing in alumina material. Thus, any improvement in the calibration slope was often counteracted by the increase in standard deviation. This difference in standard deviation can be attributed to the contrast in scale between devices for current measurements. Larger numbers tend to have a higher relative spread due to their greater scale. Even with a similar spread, larger numbers tend to result in a higher standard deviation because the absolute difference from the mean is greater due to scale differences.

4.6 Micropad Printing on Multichannel Design

The best-performing materials were printed as micropads and tested on the multi-channel design. However, the micropads were manually printed due to alignment difficulties with the screen-printer. The ZnO nanoparticle material made with either PVA or PVAc was tested.

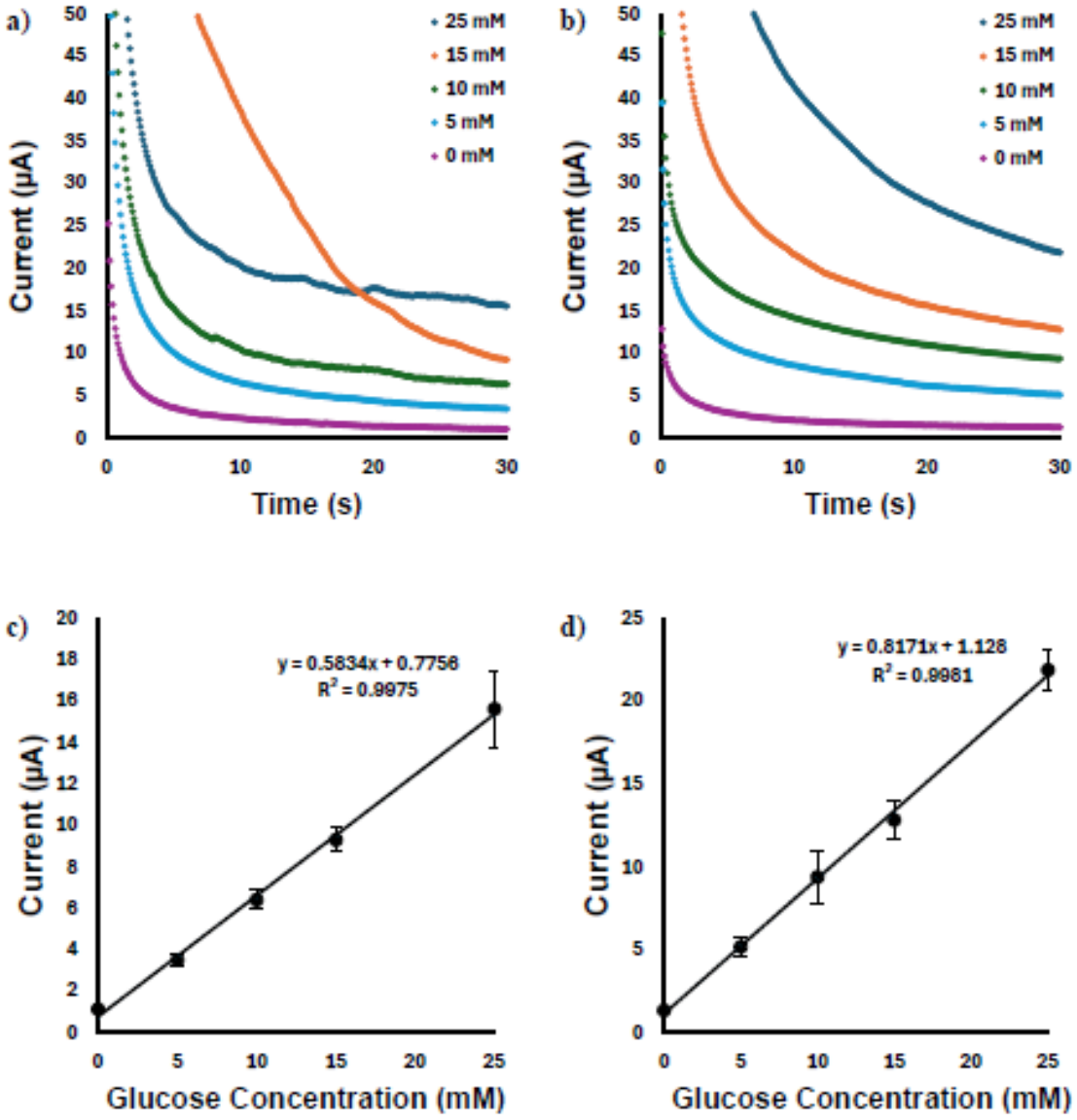

Figure 4.9: Chronoamperometric curves for glucose concentrations ranging from 0 mM to 25 mM for multichannel devices with a) ZnO nanoparticle in PVA micropads and b) ZnO nanoparticle in PVAc micropads. Calibration curves for glucose concentration as a function of current at time = 30 seconds for the same multichannel devices with c) ZnO nanoparticle in PVA micropads d) ZnO nanoparticle in PVAc micropads. Testing was done using CH Instruments CHI600D electrochemical analyzer.

Compared to previous tests using the ZnO nanoparticle material, the current signal was significantly lower. The LOD was determined to be 0.29 and 0.22 mM for the ZnO nanoparticle in PVA and PVAc, respectively. The 4M4E device has a greater surface area than the smaller multichannel electrode. The electrode's surface area difference can affect the amount of current generated during chronoamperometry. A similar phenomenon was observed in the alumina-based devices, but not to the same extent. Although the LOD did not improve, this result was still significant in demonstrating the degree of signal amplification by the semiconductor material.

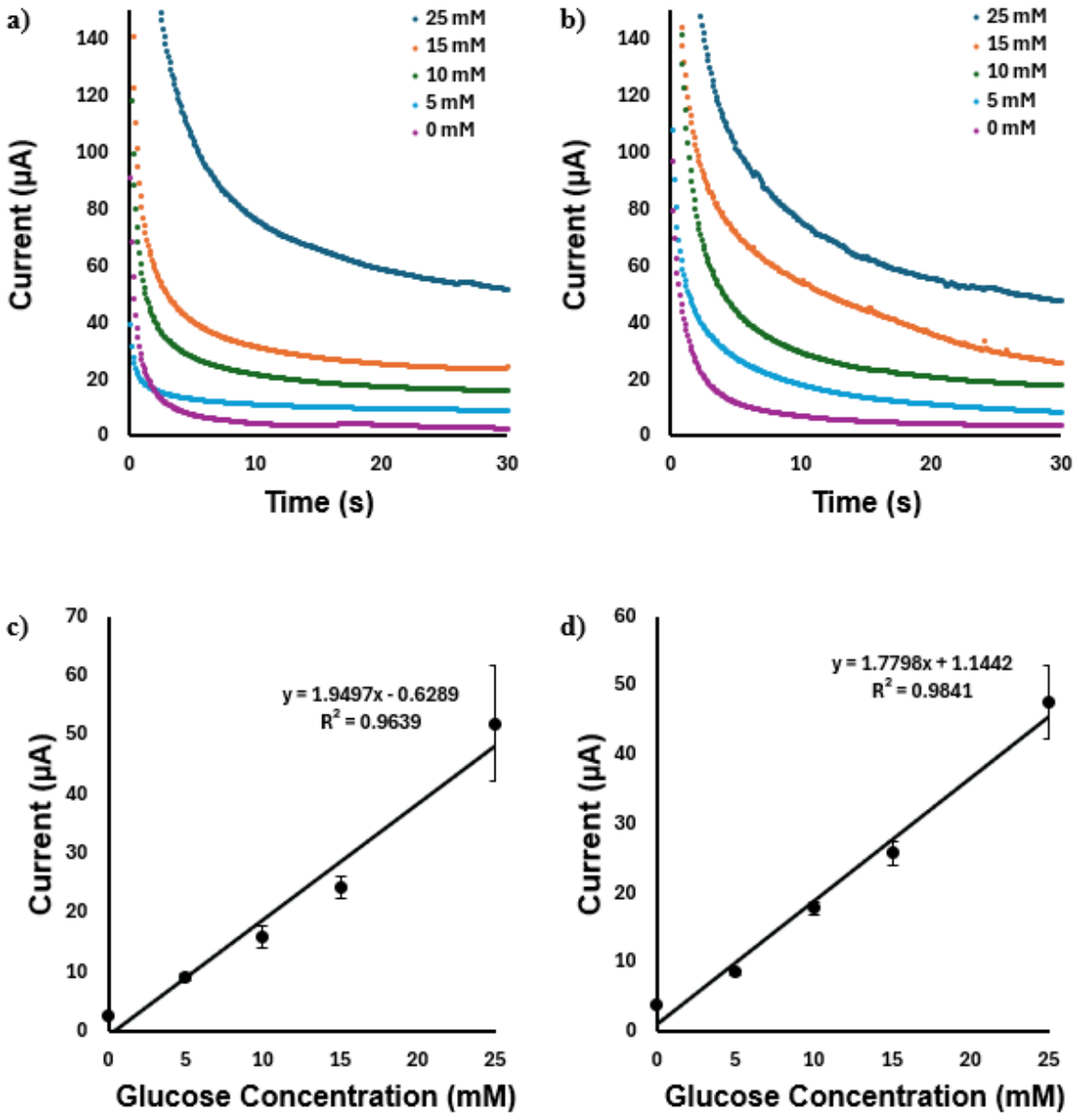

Figure 4.10: Chronoamperometric curves for glucose concentrations ranging from 0 mM to 25 mM for multichannel devices with a) 8% carbon black and b) 5% carbon black micropads. Calibration curves for glucose concentration as a function of current at time = 30 seconds for the same multichannel devices with c) 8% carbon black and d) 5% carbon black micropads. Testing was done using CH Instruments CHI600D electrochemical analyzer.

Looking at the chronoamperometric curves for the carbon black micropads, a similar trend can be seen. There are distinct current responses for each of the investigated glucose concentrations. The current signal at 30 seconds was lower, when compared to their 4M4E counterparts. The LOD for the 8% carbon black devices was 0.015 mM. The devices with 5% carbon black micropads had an LOD of 0.031 mM. The addition of carbon black resulted in higher current responses and enhanced sensitivity. Notably, the 8% carbon black micropads provided an optimal balance, maximizing sensitivity while minimizing issues for both the 4M4E and multichannel designs.

4.7 Plasma Treated Carbon Electrode

Plasma treatment is a powerful technique used to modify the surface properties of materials by exposing them to reactive oxygen species (Wang et al., 2009) (Osaki et al., 2024). After plasma treatment, it is possible to enhance the surface characteristics, such as increased surface area and improved wettability, and introduce functional groups. These surface modifications can significantly influence the electrochemical properties of the electrodes. While the purpose of plasma treatment was mainly to improve the printing of micropads onto the electrode, these side effects cannot be ignored. In this section, the potential impacts of plasma treatment on carbon electrodes are investigated, focusing on how these surface modifications can alter their chronoamperometric performance. Understanding these effects provides more insight into optimizing the electrode surface for better analytical sensing applications. The sheet of multichannel electrodes was folded to fit inside the plasma chamber. Two different conditions were tested, one at 15 seconds of plasma treatment at 0.4 mbar, with slight hints of oxidation on the reference electrode. This was referred to as

normal oxidation samples. After 30 seconds of plasma treatment, there was obvious oxidation on the entire reference electrode. This was referred to as the over-oxidation sample. These two treatments were compared to just multichannel design printed electrodes without any microfluidic layer.

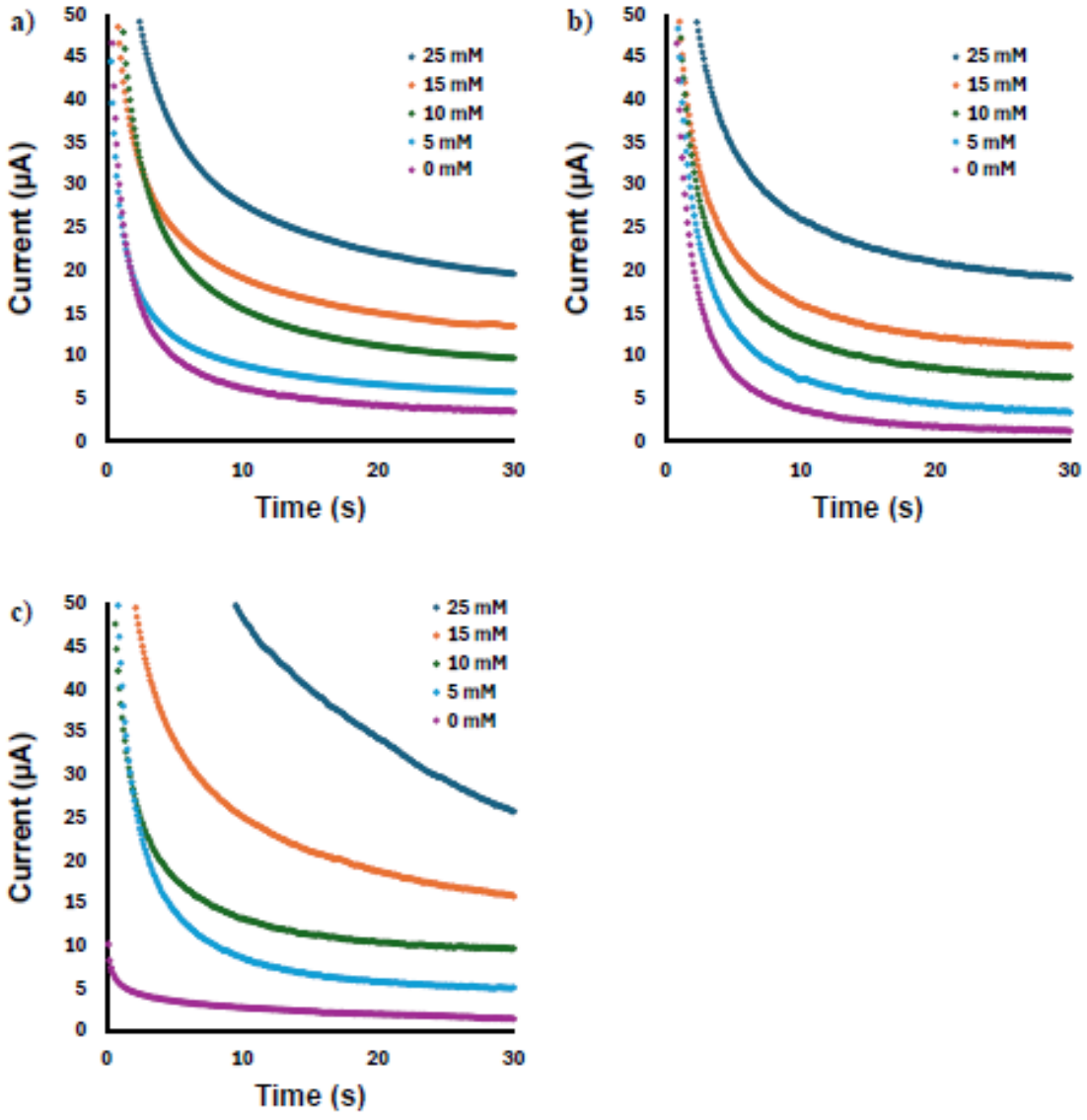

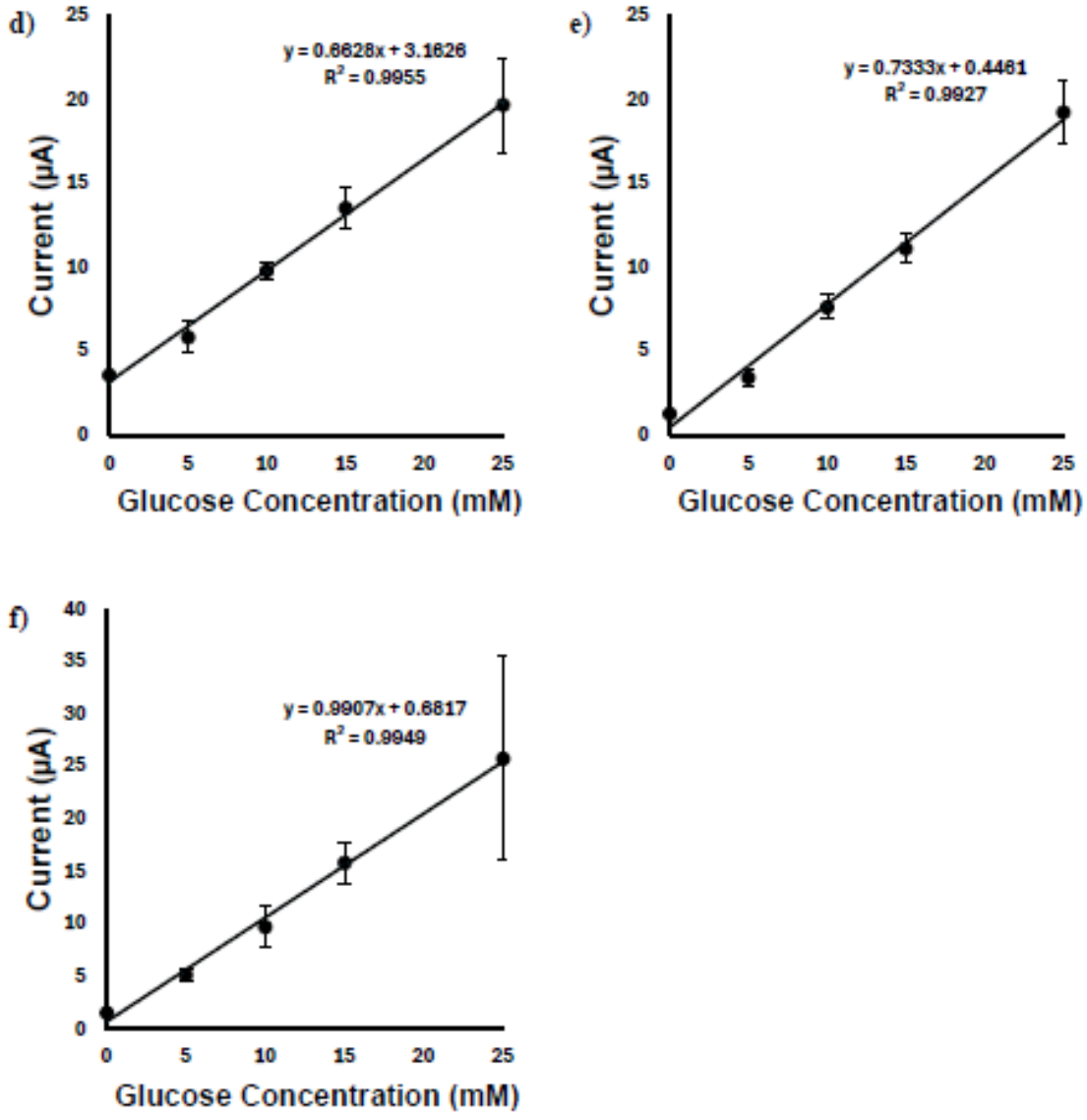

Figure 4.11: Chronoamperometric curves for glucose concentrations ranging from 0 mM to 25 mM for multichannel devices with a) no oxidation, b) normal oxidation, and c) over-oxidation. Calibration curves for glucose concentration as a function of current at time = 30 seconds for the same multichannel devices with d) no oxidation, e) normal oxidation, and f) over-oxidation. Testing was done using CH Instruments CHI600D electrochemical analyzer.

Through the process of plasma treatment, various changes to the electrode are

made that could influence its electrochemical properties, such as increased surface area and the introduction of charge to the electrode's surface. These changes contributed to the improvement in performance seen in the calibration plot, with more oxidation correlating with higher current signals. Interestingly, the standard deviation was very consistent across the treatment groups, with the change in slope being the main difference. The LOD for the no oxidation group was determined to be 0.37 mM. For normal and over oxidation, the LOD was calculated to be 0.35 and 0.26 mM, respectively. While there was not a large difference in LOD, the benefits to the electrochemical performance by plasma treatment were demonstrated, in addition to the ability to allow for easy micropad printing.

Chapter 5

Conclusion

5.1 Summary

This thesis explored the development and optimization of microfluidic devices for electrochemical glucose detection, with the main novelty being fabricating devices using a combination of alumina, ZnO and carbon black microparticles to mimic the capillarity of paper. The goal was to improve the electrochemical performance, sensitivity, and reproducibility of these devices compared to traditional paper-based microfluidics through cheap and simple solutions until they can comfortably cover the glucose concentrations found in all physiologically relevant fluids. The results demonstrated that alumina-based channels while having unfavorable electrochemical properties, were still able to display a superb performance. The mixing of ZnO with alumina saw improved performance but introduced noise and structural inconsistencies. Adding carbon black enhanced sensitivity as well but at the cost of higher standard deviation. The micropad printing technique, which localized the semiconductive material to the electrodes, provided a simple way of surface modifying the electrodes. The

best-performing devices achieved an LOD in the low micromolar range, which was a significant improvement compared to their paper-based counterparts.

This study provided insights into the behavior and performance of mixed material microfluidic channels. The integration of conductive materials such as ZnO and carbon black into an alumina matrix improved electrochemical properties but required careful control of material distribution to maintain structural integrity and consistent performance. Furthermore, the importance of surface modification to both the electrode and the microfluidic channel to the performance of the device was highlighted. The immobilization of the GOx enzyme within the microfluidic channel to prevent the washing effect or the plasma treatment of the electrodes were examples of surface modifications done to improve the performance. The fabrication process was simple, using commercially available materials and a common printing technique that allows for cost-effective and mass-producible microfluidic devices.

5.2 Limitations

Despite these advancements, there are limitations to the work. Consistency issues arose due to variability in material distribution and structural inconsistencies. While immobilization was a solution, the washing effect was never perfectly resolved. Long-term storage concerns were not thoroughly investigated. Furthermore, the devices were not tested with real samples or complex solutions with potentially interfering substances, which is crucial for practical applications. The wide glucose range used might lead to inaccurate LOD estimates, and the complicated testing procedure limits

their suitability for point-of-care applications. In several chronoamperometry experiments, a positive current signal was measured for the blank solution, suggesting some unknown reaction was not accounted for. This could affect the validity of subsequent measurements.

5.3 Future Work

Future work should further refine the microfluidic device fabrication process to improve consistency and reliability. While only a quick test was done, the microfluidic material has shown potential and capability to be integrated with commercially available screen-printed electrodes. The material can have major commercial value if further testing is done to confirm the enhancement of performance on other commercial devices and facilitate wider adoption. Comprehensive testing with real samples and potential interfering substances is necessary to validate the device's practical applicability. Investigating the device's long-term storage stability and performance will also be important. Developing more straightforward testing methods will make the device more suitable for point-of-care diagnostics. More SEM images and further testing need to be done on the fluid dynamics of the microfluidic channel to explain the fundamental differences between the pure alumina channel and alumina mixed with ZnO or carbon black channels. In conclusion, this thesis has made significant strides in developing advanced printed microfluidic devices for glucose detection, contributing a robust alternative to traditional paper-based systems. Future work should address the identified limitations and explore the broader application potential of these innovative devices.

Bibliography

Adeel, M., Rahman, M. M., Caligiuri, I., Canzonieri, V., Rizzolio, F., and Daniele, S. (2020). Recent advances of electrochemical and optical enzyme-free glucose sensors operating at physiological conditions. *Biosensors and Bioelectronics*, 165:112331.

Alahmad, W., Cetinkaya, A., Kaya, S. I., Varanusupakul, P., and Ozkan, S. A. (2023). Electrochemical paper-based analytical devices for environmental analysis: Current trends and perspectives. *Trends in Environmental Analytical Chemistry*, 40:e00220.

Amor-Gutiérrez, O., Costa-Rama, E., and Fernández-Abedul, M. T. (2022). Paper-based enzymatic electrochemical sensors for glucose determination. *Sensors*, 22:6232–6232.

Anshori, I., Harimurti, S., Rizalputri, L. N., Hartono, M. S., Althof, R. R., Handayani, M., Mengko, T. L. E. R., and Yuliarto, B. (2021). Modified screen-printed electrode using graphene ink for electrochemical sensor application. *Journal of Physics Conference Series*, 1912:012022–012022.

Anushka, Bandopadhyay, A., and Das, P. K. (2022). Paper based microfluidic devices: a review of fabrication techniques and applications. *The European Physical Journal Special Topics*, 232.

Anzar, N., Suleman, S., Bano, H., Parvez, S., Khanuja, M., Pilloton, R., and Narang, J. (2023). Paper-based electrodes decorated with silver and zinc oxide nanocomposite for electro-chemical sensing of methamphetamine. *Sensors*, 23:5519–5519.

Aruldass, S., Mathivanan, V., Mohamed, A., and Tye, C. (2019). Factors affecting hydrolysis of polyvinyl acetate to polyvinyl alcohol. *Journal of Environmental Chemical Engineering*, 7:103238.

Ataide, V. N., Mendes, L. F., Gama, L. I. L. M., Araujo, W. R. d., and Paixão, T. R. L. C. (2020). Electrochemical paper-based analytical devices: ten years of development. *Analytical Methods*, 12:1030–1054.

Bard, A. J. and Faulkner, L. R. (2000). *Electrochemical Methods: Fundamentals and Applications, 2nd Edition*. Wiley Global Education.

Barsoum, M. W. (2003). *Fundamentals of ceramics*. Institute Of Physics Publ., Cop.

Benjamin, S. R. and Miranda Ribeiro Júnior, E. J. (2022). Graphene-based electrochemical sensors for detection of environmental pollutants. *Current Opinion in Environmental Science Health*, 29:100381.

Bercea, M. (2024). Recent advances in poly(vinyl alcohol)-based hydrogels. *Polymers*, 16:2021–2021.

Cao, L., Han, G.-C., Xiao, H., Chen, Z., and Fang, C. (2020). A novel 3d paper-based microfluidic electrochemical glucose biosensor based on rgo-tepa/pb sensitive film. *Analytica Chimica Acta*, 1096:34–43.

Cate, D. M., Adkins, J. A., Mettakoonpitak, J., and Henry, C. S. (2014). Recent developments in paper-based microfluidic devices. *Analytical Chemistry*, 87:19–41.

Chaiyo, S., Mehmeti, E., Siangproh, W., Hoang, T. L., Nguyen, H. P., Chailapakul, O., and Kalcher, K. (2018). Non-enzymatic electrochemical detection of glucose with a disposable paper-based sensor using a cobalt phthalocyanine–ionic liquid–graphene composite. *Biosensors and Bioelectronics*, 102:113–120.

Charbaji, A., Heidari-Bafroui, H., Anagnostopoulos, C., and Faghri, M. (2021). Literature review of the use of zinc and zinc compounds in paper-based microfluidic devices. *Journal of Minerals and Materials Characterization and Engineering*, 9:257–270.

Chen, L., Xie, W., Luo, Y., Ding, X., Fu, B., Gopinath, S. C., and Xiong, Y. (2021). Sensitive silica-alumina modified capacitive non-faradaic glucose sensor for gestational diabetes. *Biotechnology and Applied Biochemistry*, 69:840–847.

Cinti, S., Cusenza, R., Moscone, D., and Arduini, F. (2018). Paper-based synthesis of prussian blue nanoparticles for the development of whole blood glucose electrochemical biosensor. *Talanta*, 187:59–64.

Colozza, N., Caratelli, V., Moscone, D., and Arduini, F. (2021). Origami paper-based electrochemical (bio)sensors: State of the art and perspective. *Biosensors*, 11:328.

Costa-Rama, E. and Fernández-Abedul, M. T. (2021). Paper-based screen-printed electrodes: A new generation of low-cost electroanalytical platforms. *Biosensors*, 11:51.

Cánovas, R., Parrilla, M., Blondeau, P., and Andrade, F. J. (2017). A novel wireless paper-based potentiometric platform for monitoring glucose in blood. *Lab on a Chip*, 17:2500–2507.

de Freitas, S., de Souza, F. R., Rodrigues Neto, J. C., Vasconcelos, G. A., Abdelnur, P. V., Vaz, B. G., Henry, C. S., and Coltro, W. K. (2018). Uncovering the formation of color gradients for glucose colorimetric assays on microfluidic paper-based analytical devices by mass spectrometry imaging. *Analytical Chemistry*, 90:11949–11954.

Dungchai, W., Chailapakul, O., and Henry, C. S. (2009). Electrochemical detection for paper-based microfluidics. *Analytical Chemistry*, 81:5821–5826.

Elgrishi, N., Rountree, K. J., McCarthy, B. D., Rountree, E. S., Eisenhart, T. T., and Dempsey, J. L. (2017). A practical beginner's guide to cyclic voltammetry. *Journal of Chemical Education*, 95:197–206.

Fava, E. L., Silva, T. A., Prado, T. M. d., Moraes, F. C. d., Faria, R. C., and Fatibello-Filho, O. (2019). Electrochemical paper-based microfluidic device for high throughput multiplexed analysis. *Talanta*, 203:280–286.

Gentile, K., Maiti, S., Brink, A., Rallabandi, B., Stone, H. A., and Sen, A. (2020). Silver-based self-powered ph-sensitive pump and sensor. *Langmuir*, 36:7948–7955.

Gong, M. M. and Sinton, D. (2017). Turning the page: Advancing paper-based microfluidics for broad diagnostic application. *Chemical Reviews*, 117:8447–8480.

Gutiérrez-Capitán, M., Baldi, A., and Fernández-Sánchez, C. (2020). Electrochemical paper-based biosensor devices for rapid detection of biomarkers. *Sensors*, 20:967.

Hassan, M. H., Vyas, C., Grieve, B., and Bartolo, P. (2021). Recent advances in enzymatic and non-enzymatic electrochemical glucose sensing. *Sensors*, 21:4672.

Kant, T., Shrivas, K., Tapadia, K., Devi, R., Ganesan, V., and Deb, M. K. (2021). Inkjet-printed paper-based electrochemical sensor with gold nano-ink for detection of glucose in blood serum. *New Journal of Chemistry*, 45:8297–8305.

Kava, A. A. and Henry, C. S. (2021). Exploring carbon particle type and plasma treatment to improve electrochemical properties of stencil-printed carbon electrodes. *Talanta*, 221:121553.

Kong, F.-Y., Gu, S.-X., Li, W.-W., Chen, T.-T., Xu, Q., and Wang, W. (2014). A paper disk equipped with graphene/polyaniline/au nanoparticles/glucose oxidase biocomposite modified screen-printed electrode: Toward whole blood glucose determination. *Biosensors and Bioelectronics*, 56:77–82.

Kołodziejczak-Radzimska, A. and Jesionowski, T. (2014). Zinc oxide—from synthesis to application: A review. *Materials*, 7:2833–2881.

Kulkarni, M. B., Ayachit, N. H., and Aminabhavi, T. M. (2022). Biosensors and microfluidic biosensors: From fabrication to application. *Biosensors*, 12:543.

Kumar, S., Pandey, C. M., Hatamie, A., Simchi, A., Willander, M., and Malhotra, B. D. (2019). Nanomaterial-modified conducting paper: Fabrication, properties, and emerging biomedical applications. *Global challenges*, 3.

Lamas-Ardisana, P., Martínez-Paredes, G., Añorga, L., and Grande, H. (2018). Glucose biosensor based on disposable electrochemical paper-based transducers fully fabricated by screen-printing. *Biosensors and Bioelectronics*, 109:8–12.

Lankelma, J., Nie, Z., Carrilho, E., and Whitesides, G. M. (2012). Paper-based analytical device for electrochemical flow-injection analysis of glucose in urine. *Analytical Chemistry*, 84:4147–4152.

Lee, W., Kang, T., Kim, S.-H., and Jeong, J. (2018). An antibody-immobilized silica inverse opal nanostructure for label-free optical biosensors. *Sensors*, 18:307.

Li, W., Qian, D., Wang, Q., Li, Y., Bao, N., Gu, H., and Yu, C. (2016). Fully-drawn origami paper analytical device for electrochemical detection of glucose. *Sensors and Actuators B: Chemical*, 231:230–238.

Li, X., Ballerini, D. R., and Shen, W. (2012). A perspective on paper-based microfluidics: Current status and future trends. *Biomicrofluidics*, 6:11301–1130113.

Li, X., Zhao, C., and Liu, X. (2015). A paper-based microfluidic biosensor integrating zinc oxide nanowires for electrochemical glucose detection. *Microsystems Nanoengineering*, 1.

Li, Z., Li, F., Xing, Y., Liu, Z., You, M., Li, Y., Wen, T., Qu, Z., Ling Li, X., and Xu, F. (2017). Pen-on-paper strategy for point-of-care testing: Rapid prototyping of fully written microfluidic biosensor. *Biosensors and Bioelectronics*, 98:478–485.

Manasa, G., Mascarenhas, R. J., Shetti, N. P., Malode, S. J., Mishra, A., Basu, S., and Aminabhavi, T. M. (2022). Skin patchable sensor surveillance for continuous glucose monitoring. *ACS Applied Bio Materials*, 5:945–970.

Martinez, A., Phillips, S., Butte, M., and Whitesides, G. (2007). Patterned paper as a platform for inexpensive, low-volume, portable bioassays. *Angewandte Chemie*, 119:1340–1342.

Mettakoonpitak, J., Boehle, K., Nantaphol, S., Teengam, P., Adkins, J. A., Srisa-Art, M., and Henry, C. S. (2016). Electrochemistry on paper-based analytical devices: A review. *Electroanalysis*, 28:1420–1436.

Nanja, A. F., Focke, W. W., and Musee, N. (2020). Aggregation and dissolution of aluminium oxide and copper oxide nanoparticles in natural aqueous matrixes. *SN Applied Sciences*, 2.

Niamsi, W., Larpant, N., Kalambate, P. K., Primpray, V., Karuwan, C., Rodthongkum, N., and Laiwattanapaisal, W. (2022). Paper-based screen-printed ionic-liquid/graphene electrode integrated with prussian blue/mxene nanocomposites enabled electrochemical detection for glucose sensing. *Biosensors*, 12:852–852.

Nie, Z., Deiss, F., Liu, X., Akbulut, O., and Whitesides, G. M. (2010a). Integration of paper-based microfluidic devices with commercial electrochemical readers. *Lab on a Chip*, 10:3163–3169.

Nie, Z., Nijhuis, C. A., Gong, J., Chen, X., Kumachev, A., Martinez, A. W., Narovlyansky, M., and Whitesides, G. M. (2010b). Electrochemical sensing in paper-based microfluidic devices. *Lab Chip*, 10:477–483.

Noiphung, J., Songjaroen, T., Dungchai, W., Henry, C. S., Chailapakul, O., and Laiwattanapaisal, W. (2013). Electrochemical detection of glucose from whole blood using paper-based microfluidic devices. *Analytica Chimica Acta*, 788:39–45.

Novaković, T., Barudžija, T., Čomor, M., Banković, P., and Mojović, Z. (2021). Electrochemical behavior of different types of alumina. *Journal of Electroanalytical Chemistry*, 895:115542–115542.

Osaki, S., Saito, M., Nagai, H., and Tamiya, E. (2024). Surface modification of screen-printed carbon electrode through oxygen plasma to enhance biosensor sensitivity. *Biosensors*, 14:165–165.

Paimard, G., Ghasali, E., and Baeza, M. (2023). Screen-printed electrodes: Fabrication, modification, and biosensing applications. *Chemosensors*, 11:113.

Parrilla, M., Cánovas, R., and Andrade, F. J. (2017). Paper-based enzymatic electrode with enhanced potentiometric response for monitoring glucose in biological fluids. *Biosensors and Bioelectronics*, 90:110–116.

Pullano, S. A., Greco, M., Bianco, M. G., Foti, D., Brunetti, A., and Fiorillo, A. S. (2022). Glucose biosensors in clinical practice: principles, limits and perspectives of currently used devices. *Theranostics*, 12:493–511.

Rackus, D. G., Shamsi, M. H., and Wheeler, A. R. (2015). Electrochemistry, biosensors and microfluidics: a convergence of fields. *Chemical Society Reviews*, 44:5320–5340.

Radhakrishnan, S., Lakshmy, S., Santhosh, S., Kalarikkal, N., Chakraborty, B., and Rout, C. S. (2022). Recent developments and future perspective on electrochemical glucose sensors based on 2d materials. *Biosensors*, 12:467.

Rezaei, R., Foroughi, M. M., Beitollahi, H., and Alizadeh, R. (2018). Electrochemical sensing of uric acid using a zno/graphene nanocomposite modified graphite screen printed electrode. *Russian Journal of Electrochemistry*, 54:860–866.

Rock, P. A. (1966). The standard oxidation potential of the ferrocyanide-ferricyanide

electrode at 25° and the entropy of ferrocyanide ion. *The Journal of Physical Chemistry*, 70:576–580.

Shangguan, J.-W., Liu, Y., Wang, S., Hou, Y.-X., Xu, B.-Y., Xu, J.-J., and Chen, H.-Y. (2018). Paper capillary enables effective sampling for microfluidic paper analytical devices. *ACS Sensors*, 3:1416–1423.

Shen, L., Zhang, G., and Etzold, B. J. M. (2019). Paper-based microfluidics for electrochemical applications. *ChemElectroChem*, 7:10–30.

Sinha, L., Lee, H., Ohshita, Y., and Shirage, P. M. (2020). Defect mediated w¡sub¿18¡/sub¿o¡sub¿49¡/sub¿ nanorods bundle for nonenzymatic amperometric glucose sensing application. *ACS Biomaterials Science Engineering*, 6:1909–1919.

Squillace, O., Fong, R., Shepherd, O., Hind, J., Tellam, J., Steinke, N.-J., and Thompson, R. L. (2020). Influence of pvac/pva hydrolysis on additive surface activity. *Polymers*, 12:205.

Tortorich, R., Shamkhalichenar, H., and Choi, J.-W. (2018). Inkjet-printed and paper-based electrochemical sensors. *Applied Sciences*, 8:288.

Van, E. A., Ximenes, E. S., Tarasconi, L. T., Teresinha, I., Madalena, M., and Boudinov, H. I. (2014). Insulating characteristics of polyvinyl alcohol for integrated electronics. *Thin Solid Films*, 568:111–116.

Wang, J. (2008). Electrochemical glucose biosensors. *Elsevier eBooks*, pages 57–69.

Wang, S., Chang, K., and Yuan, C. (2009). Enhancement of electrochemical properties of screen-printed carbon electrodes by oxygen plasma treatment. *Electrochimica Acta*, 54:4937–4943.

Witkowska Nery, E., Kundys, M., Jeleń, P. S., and Jönsson-Niedziółka, M. (2016). Electrochemical glucose sensing: Is there still room for improvement? *Analytical Chemistry*, 88:11271–11282.

Wu, Y., Ren, Y., Han, L., Yan, Y., and Jiang, H. (2019). Three-dimensional paper based platform for automatically running multiple assays in a single step. *Talanta*, 200:177–185.

Xu, J., Yan, Z., and Liu, Q. (2022). Smartphone-based electrochemical systems for glucose monitoring in biofluids: A review. *Sensors*, 22:5670.

Xu, Y., Liu, M., Kong, N., and Liu, J. (2016). Lab-on-paper micro- and nano-analytical devices: Fabrication, modification, detection and emerging applications. *Microchimica Acta*, 183:1521–1542.

Yamada, K., Shibata, H., Suzuki, K., and Citterio, D. (2017). Toward practical application of paper-based microfluidics for medical diagnostics: state-of-the-art and challenges. *Lab on a Chip*, 17:1206–1249.

Yao, Y. and Zhang, C. (2016). A novel screen-printed microfluidic paper-based electrochemical device for detection of glucose and uric acid in urine. *Biomedical Microdevices*, 18.

Yoo, E.-H. and Lee, S.-Y. (2010). Glucose biosensors: An overview of use in clinical practice. *Sensors*, 10:4558–4576.

Zhang, H., Xia, C., Feng, G., and Fang, J. (2021). Hospitals and laboratories on paper-based sensors: A mini review. *Sensors*, 21:5998–5998.

Zhang, Z., Lang, S., Pearson, K., Farhan, Y., Tao, Y., and Xiao, G. (2023). Printed capillary microfluidic devices and their application in biosensing. *Micromachines*, 14:2059–2059.

Zhao, C., Thuo, M. M., and Liu, X. (2013). A microfluidic paper-based electrochemical biosensor array for multiplexed detection of metabolic biomarkers. *Science and Technology of Advanced Materials*, 14:054402.

Zheng, W., Wang, K., Xu, H., Zheng, C., Cao, B., Qin, Q., Jin, Q., and Cui, D. (2021). Strategies for the detection of target analytes using microfluidic paper-based analytical devices. *Analytical and Bioanalytical Chemistry*, 413:2429–2445.